



Article

Petrology of Granites of the Tommot Rare-Earth Ore Field (Verkhoyansk–Kolyma Orogenic Belt)

Vera A. Trunilina  and Andrei V. Prokopiev 

Diamond and Precious Metal Geology Institute, Siberian Branch of Russian Academy of Sciences, Lenin Av. 39, Yakutsk 677980, Russia

* Correspondence: trunilina40@mail.ru; Tel.: +7-9141016992

Abstract: The article presents the results of studying the aegirine–arfvedsonite granites of the Somnitelnyi massif within the Tommot ore field located in the Verkhoyansk–Kolyma orogenic belt (NE Asia). Along with the crustal signatures, the rocks display features of mantle contamination at their origin. Their affinity for A-type granites characteristic of continental rifts and hot spots is shown. The associated Tommot REE deposit is the only one discovered in NE Russia. New data are presented for the previously studied Tommot massif within the same ore field, with a wide compositional range from alkaline-ultrabasic rocks to alkaline syenites. It is established that despite a common geochemical enrichment of both massifs' rocks with REEs, the Somnitelnyi massif granites cannot be interpreted as the final phase of the Tommot massif emplacement. Specific REE mineralization and high crystallization temperatures (up to 1045 °C) of the Somnitelnyi granites may be explained by the existence within the study area of an undepleted mantle source (“hot spot”), whose maximum activity occurred during the granitic melt generation. The ore bodies of the Tommot deposit consist of fenitized albitites, granite gneisses, and, more rarely, the cross-cutting pegmatite veins. They are confined mostly to exocontacts of the Somnitelnyi massif, are less often in its endocontacts, and are not found in the host rocks and in the inner part of the massif away from the contacts. Principal ore minerals are chevkinite, yttrialite, gadolinite, and fergusonite. Based on the data obtained, the deposit is classified as a metasomatic complex Ce–Y–Nb–Zr deposit associated with the alkaline granites.

Keywords: REE mineralization; A-type granites; petrography; mineralogy; geochemistry; petrology; Verkhoyansk–Kolyma orogenic belt



Citation: Trunilina, V.A.; Prokopiev, A.V. Petrology of Granites of the Tommot Rare-Earth Ore Field (Verkhoyansk–Kolyma Orogenic Belt). *Minerals* **2022**, *12*, 1347. <https://doi.org/10.3390/min12111347>

Academic Editor: Clemente Recio

Received: 18 July 2022

Accepted: 19 October 2022

Published: 24 October 2022

Publisher's Note: MDPI stays neutral with regard to jurisdictional claims in published maps and institutional affiliations.



Copyright: © 2022 by the authors. Licensee MDPI, Basel, Switzerland. This article is an open access article distributed under the terms and conditions of the Creative Commons Attribution (CC BY) license (<https://creativecommons.org/licenses/by/4.0/>).

1. Introduction

Rare-earth elements (REEs) belong to the so-called “critical” or strategic metals due to their wide application both in the civil and defense industries. Therefore, it is natural that many researchers take an active interest in them. Due to the rapid development of technological progress around the world, the demand for REEs is growing rapidly too.

There are numerous classifications of REE deposits [1–4], but traditionally, they have been divided into three wide groups: (a) magmatic REE deposits associated with carbonatites and alkaline magmatic complexes, REE–U–Nb pegmatites, REE-bearing hydrothermal iron deposits, and Be- and Y-bearing alkaline intrusive rocks (nepheline syenites); (b) REE–F–Ba–Th vein deposits; and (c) sedimentary REE–(Ti–P–Nb) deposits including alluvial and beach placers, REE-bearing phosphorites, ion-adsorption clays, and REE-bearing coals. The authors adhere to the classification proposed by N.V. Eremin [5]: magmatic deposits, deposits related to feldspar metasomatites, carbonatites, ion-adsorption clays, littoral-marine placers, sedimentary phosphate rocks, and organogenic phosphate rocks. In the view of most researchers, the alkaline rocks and carbonatites are the most productive for rare-earth elements [6].

Russia has a large raw material base for REEs, making up 16.5% of the world's reserves. Here, as all over the world, prevalent REE deposits are related to carbonatites, alkaline

rocks, and metasomatites (Belaya Zima, Lovozero, Chuktukonskoye, Katuginskoye, Zashikhinskoye, etc.). Within the Republic of Sakha (Yakutia), most of the REE reserves are concentrated in carbonatite-related deposits: the Tomtor deposit on the eastern slope of the Anabar Shield, Seligdar in the Aldan Shield, and Gornoe Ozero in West Verkhoyansk. In the north-east of the republic, there is known of only one Tommot REE deposit within the Tommot ore field and a series of mineralization points. All of them are associated with granites, tentatively classified by the author of [7] as A-type. A-type granites have long been known as possible sources of rare-metal and REE mineralization [8–12]. They range widely in their petro- and geochemical composition, as does the related mineralization. The genesis of such granites is a matter of debate. Some authors believe they are the result of the syntaxis of mantle and crustal melts [9,13,14], others consider them the late differentiates of crustal granitoid melts [15,16], and still others interpret them to be differentiates of mantle magmas [17,18]. Specialized prospecting works for REEs, with the accompanying mine workings, were carried out only at the Tommot deposit in the 1950s and 1960s of the 20th century. New targets within the Selennyakh and Uyandina river basin area were not examined in detail and not evaluated. Petrography and geochemistry of the granitoids associated with REE mineralization were not thoroughly investigated, no classification of REE occurrences in the study area was developed, and the processes of their generation were not studied. The objective of this work was to establish the genesis of the granites accompanied by the Tommot REE deposit and to identify the formation type of mineralization.

2. Methods

During field studies, the structure of magmatic bodies and localization of mineralization were determined. Petrography of the granitoids and ores was studied with the use of an Olympus optical microscope (Leica, Germany), enabling determination of the crystallization and evolution paths of the melts.

The compositions of the rock-forming and accessory minerals were analyzed using a Camebax-Micro X-ray microanalyzer (Cameca, Courbevoie, France). The analytical conditions were: accelerating voltage, 20 kV; beam current, 1.08 nA; counting time, 10 s; detection limits, 0.01%; reproducibility, 0.15–0.2.

Feldspars were studied using optical methods with a Fedorov universal stage (the Fedorov method) [19], allowing the determination of zoning patterns and the structural ordering of minerals. The Fedorov method involves determining the shape and orientation of the optical indicatrix in a crystal. The degree of structural (or crystal) ordering is defined as the amount of deviation of the real (observed) spatial lattice of a crystal from the ideal (theoretical) spatial lattice, which tends to decrease with increasing temperature [20].

All analyses except ICP–MS were conducted at the Diamond and Precious Metal Geology Institute (DPMGI SB RAS), Yakutsk, Russia. Samples for analytical studies were prepared using standard crushing and grinding procedures. The mineral grains were separated by magnetic and density separation with final sorting under a binocular microscope to remove altered grains and other random minerals, and then, were crushed to 200 mesh. The chemical compositions of the rocks were determined using a conventional wet-chemistry analytical technique. They are given in Tables S1–S5.

The REE content in the rocks was determined by ICP–MS analysis on a high-resolution ELEMENT 2 mass spectrometer (ThermoQuest Finnigan MAT, Germany) at the Geochemistry Institute, SB RAS (Irkutsk). Detection limits for the analyzed elements (ppm): La—6.2, Ce—0.44, Pr—0.027, Nd—0.07, Sm—0.018, Eu—0.014, Gd—0.037, Tb—0.015, Dy—0.015, Ho—0.009, Er—0.035, Tm—0.0063, Yb—0.014, Lu—0.047, Hf—0.1, Ta—0.18, Y—0.24, Zr—1.48, Be—0.08, Th—0.11, U—0.037; reproducibility—0.1–0.3.

Trace elements were detected using a PGS-2 spectrograph equipped with a multichannel atomic emission spectral analyzer (BMK Optoelectronics, Russia). A sample mixed with a refractory buffer was vaporized from the carbon electrode channel filled with an internal standard. The buffer for the atomic emission analysis of volatile elements is a

mixture of 7 weight fractions of Al_2O_3 , 3 fractions of CaCO_3 , 1 fraction of K_2CO_3 , and 0.02% Bi_2O_3 . The buffer for carbonates consists of 5 weight fractions of Al_2O_3 , 4 fractions of SiO_2 , 1 fraction of K_2CO_3 , and 0.02% Bi_2O_3 . Standards and samples were diluted with a buffer in the optimal weight ratio of 1:2. The buffer for the Fe-group elements was 0.05% of the internal standard mixed with carbon powder to ensure uniform evaporation of the sample. The buffer-to-sample weight ratio was 1:1. Based on the results of standard burning, diagrams were constructed to help determine the content of the analyzed elements. To correct variations in the position of the spectrum, we used reference lines (Pd 302.79 nm and 342 nm). Detection limits (ppm) are: Ba—19, Sr—6, Cr—13, Ni—4, V—5, Co—1.3, Zr—23, Nb—8, Y—5, Yb—0.5; reproducibility—0.1–0.2.

A complete whole-rock geochemical analysis and spectral analysis of REEs and trace elements in the ores were performed, followed by mathematical processing of the data using CGDkit, PetroExplorer software [21,22].

3. Geological Setting

The Verkhoyansk–Kolyma orogenic belt represents a collage of terranes of various affinity [23,24] (Figure 1). The Tommot ore field is localized in the northern part of the Omulevka terrane, which is interpreted as a fragment of the Siberian craton. It is assumed to have been detached from the craton as a result of Devonian rifting and reconnected with it due to the Verkhoyansk orogeny at the beginning of the Cretaceous [23,24]. The terrane is divided into several blocks. One of the largest is the Selennyakh block, wherein the Tommot ore field occurs. Here, among the Middle Ordovician shallow carbonate rocks lies a tectonic sheet of presumably Proterozoic schists interbedded with para- and orthoamphibolites, marbles, and granite gneisses (Figure 2). Some researchers interpret these metamorphic rocks as part of an ophiolitic complex [23,24].

The data on the isotopic age of the schists are contradictory. The ^{39}Ar – ^{40}Ar method dates the amphibole schists as Early Devonian (415 Ma, whole rock), whereas actinolite and tremolite from them are determined as Proterozoic (640 and ca. 900 Ma, respectively) [25]. P. Layer et al. do not think the latter age determinations to be reliable because of low contents of K and radiogenic Ar in actinolite and tremolite [25]. However, Rb–Sr ages of the amphibole and biotite–amphibole schists are 622 and 555 Ma, respectively, and the K–Ar age of chlorite schists is 655 Ma [26]. These data show that the possibility of a Proterozoic age of the schists must not be ruled out.

The Tommot ore field includes the Tommot REE deposit localized in the contacts of alkaline granites of the Somnitelnyi massif, with host rocks and minor REE occurrences in the Tommot massif syenites (Figure 3).

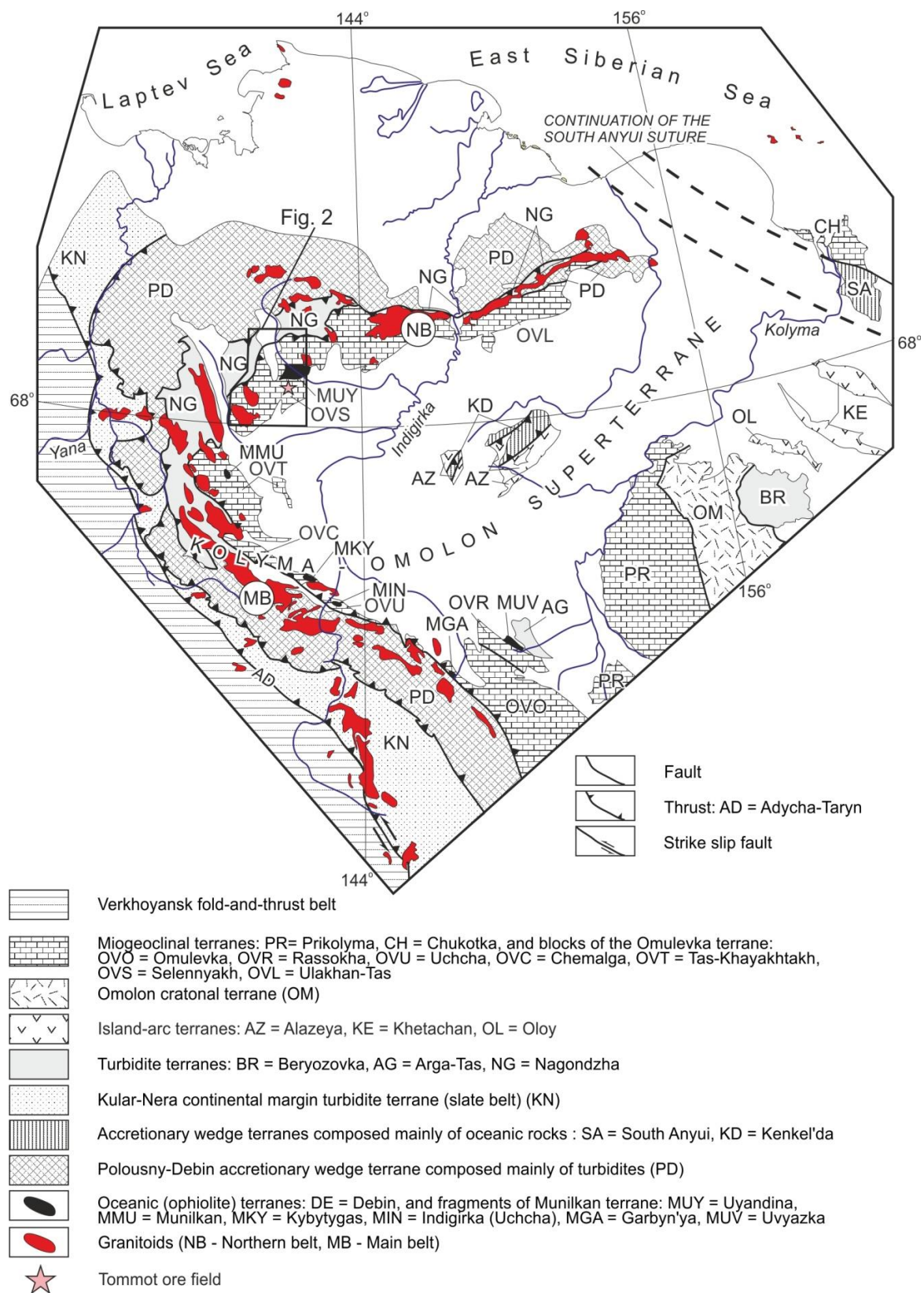


Figure 1. Tectonic map of the northeastern Verkhoyansk–Kolyma orogenic belt [modified 23].

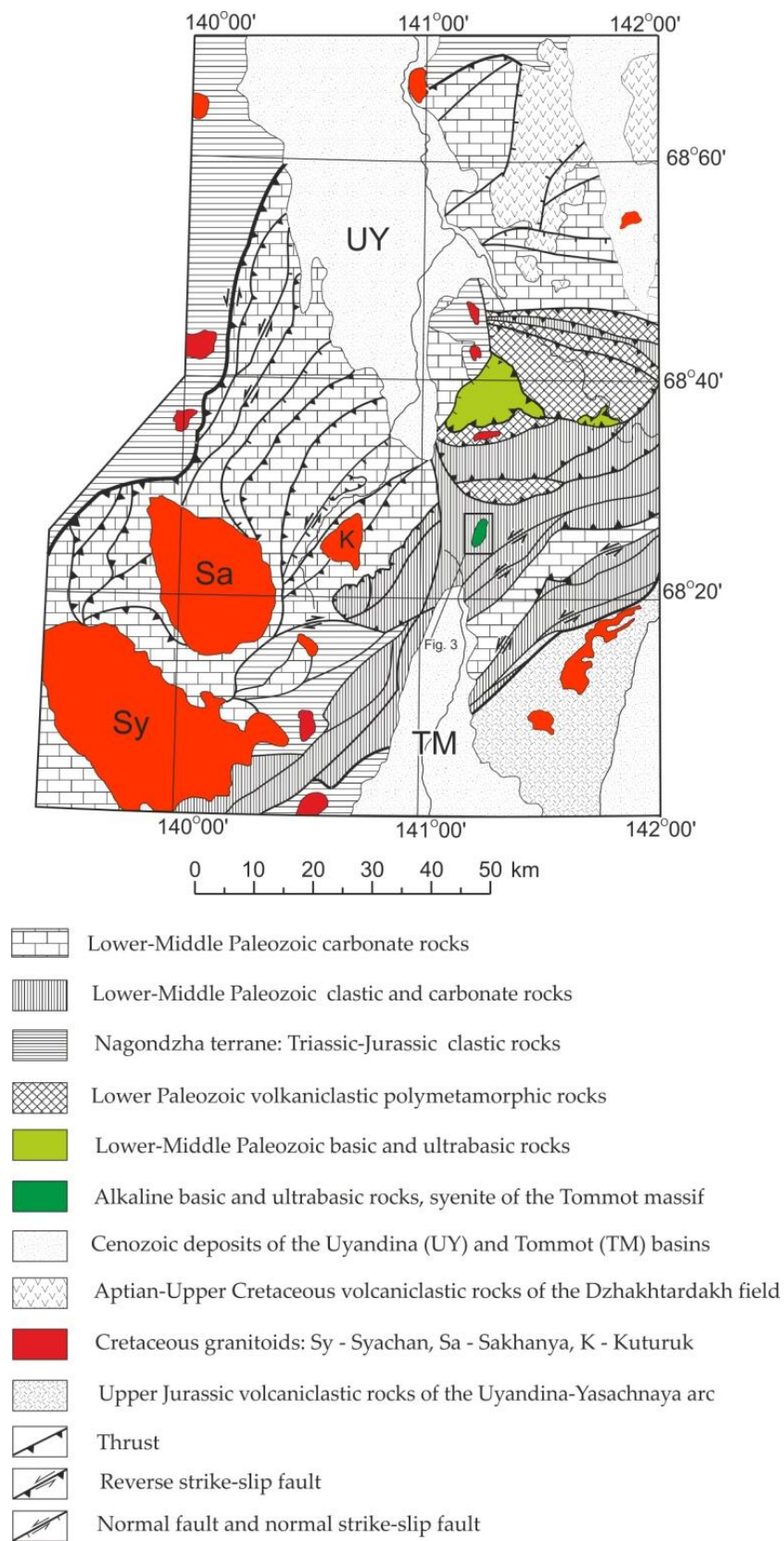


Figure 2. Geological sketch map of the Selennyakh block of the Omulevka terrane [modified 23]. For location, see Figure 1.

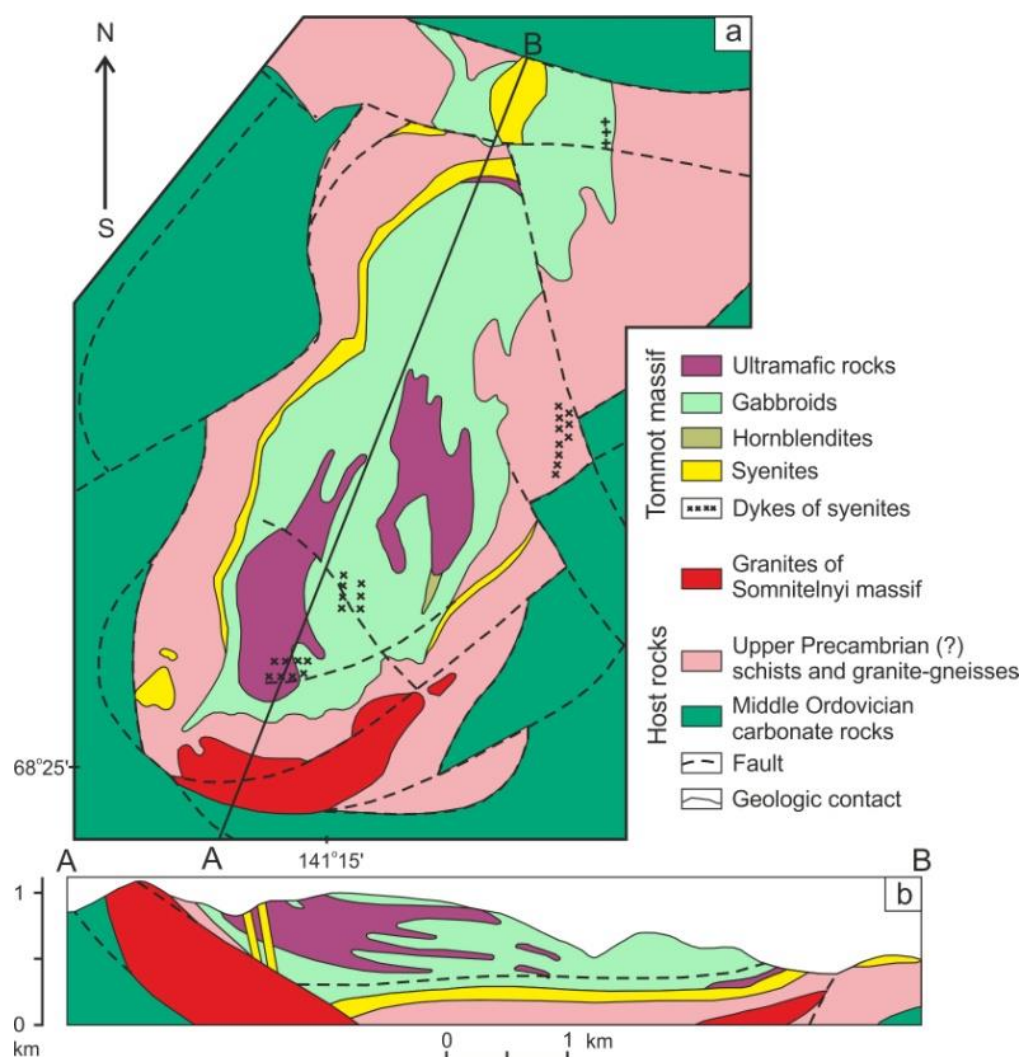


Figure 3. (a) Schematic map of the Tommot and Somnitelnyi massifs; (b) geological cross-section (A,B) (modified from [27]). For location, see Figure 2.

The Tommot deposit was discovered in 1954–1955, when several ore bodies with Th and REE mineralization were found during the verification of radiometric anomalies. The deposit is classed as an Y-group REE deposit related to pegmatites [28]. In 1991–1993, under the guidance of the first author, workers of the IGABM SB RAS and the Yakut State Prospect-and-Survey Expedition conducted a study of magmatism and composition of major ore bodies in order to improve the predictive estimation of the deposit potential. As a result, the geological structure of the Tommot massif was more precisely defined, and the main ore bodies were characterized. In 2007–2009, the magmatic and host rocks of the ore field were sampled to determine their age [27]. During geological mapping, the structure and parameters of the ore bodies were clarified [29]. However, the mineralogy, geochemistry, and genetic features of granitoids within the ore field were poorly studied.

Within the Tommot ore field, para- and orthoamphibolites, variably fenitized granite gneisses, schists, and interlayers of skarnified rocks, marbles, and limestones are observed. They are intruded by the multiphase Tommot massif of alkaline rocks of varying composition and the Somnitelnyi massif of alkaline granites and leucogranites to the south of it (Figure 3). Both the host rocks and the Tommot massif are cut by numerous NE-directed faults. It is probably along these fault zones that the introduction of a granitic melt took place.

The Tommot massif is composed of alkaline-ultrabasic rocks, alkaline and subalkaline gabbro, and alkaline syenites (Figure 3). The alkaline-ultrabasic rocks (feldspar-free ore jacupirangites, feldspar jacupirangites, and melanocratic gabbroids) form gently dipping bodies with a thickness up to 500 m, stretching north-easterly for a distance of up to 2.5 km. As a result of intense postintrusive tectonic processes, they were divided into separate blocks. The alkaline and subalkaline gabbro, feldspathoid essexites, and theralites form a lenticular body elongated in the N–S direction, with an outcrop area of 12 km² and a thickness up to 1 km. They contain numerous xenoliths of alkaline-ultrabasic rocks. At the contacts with syenites, the gabbroids are brecciated, gneissic, and cemented together with the host rocks by syenite material. The alkaline syenites compose a plate-like body in the western exocontact of the gabbroid massif. It is 30–100 m thick, has a N–S strike, and dips to the east at angles of 40–60°. The syenites are also strongly broken down. Some thin, steeply dipping dykes of pegmatoid alkaline syenites cut both the gabbroids and the ultrabasic rocks.

The alkaline granites of the Somnitelnyi massif form the apical part of a steeply inclined plate-like body interrupting the schists and gabbroids of the Tommot massif (Figure 3). The southern contact of the Somnitelnyi massif is confined to the zone of a large W–E fault, along which the contact-metamorphosed schists overlie the Ordovician carbonate rocks. The southern and northern contacts dip to the north at angles of 70–80° and 40–60°, respectively, cutting foliation of the host rocks. Along the fault, the host rocks are badly broken down and gneissic. In the apical part of the massif, the orientation of the contact surface is subhorizontal, which is subconformable with the host rocks.

Ore bodies within the Tommot deposit are represented by quartz albitite veins as thick as 0.3–2.8 m with an REE mineral content of 0.3%–3.2%, and are cut by quartz–microcline pegmatites and quartz veins with nests of aegirine and arfvedsonite in association with the same REE minerals, such as albitites, whose content in some areas amounts to 10%–20%. Mineralization mostly occurs either close to the exocontact or nearby the xenoliths and xenoblocks of the host rocks in the endocontact of the granite massif. No mineralization is found in a highly eroded part of the granite massif and in the host rocks away from the contacts. The major ore body of the deposit is localized along the contact of the granites with biotite–amphibole schists interbedded with feldspar–amphibole and quartz–feldspar–amphibole schists and limestones.

The isotopic age of magmatic rocks within the Tommot ore field is discussed in detail in [27]. The alkaline-ultrabasic rocks of the Tommot massif were estimated by the K–Ar method at 367–398 Ma. The ³⁹Ar–⁴⁰Ar dating of hornblende from pyroxenite yielded 340 Ma. The isotopic age of alkaline gabbro is, according to the ³⁹Ar–⁴⁰Ar method, 300 Ma, and according to the Rb–Sr method, 329 ± 29 Ma. As determined by ³⁹Ar–⁴⁰Ar dating, alkaline syenites have an age close to that of gabbro, about 300 Ma, and the Rb–Sr isochron estimated their age at 280 ± 18 Ma. For a small quartz syenite dyke from the eastern exocontact of the gabbroid massif, the Rb–Sr isochron age is 206 ± 13 Ma. The age of the Somnitelnyi granites was estimated by the Rb–Sr isochron to be 166 ± 19 Ma, while according to ³⁹Ar–⁴⁰Ar dating, they are 141 ± 0.7 Ma old.

4. Petrography and Mineralogy of Magmatic Rocks

4.1. Tommot Massif

The petrography and mineralogy of the Tommot massif rocks are described in sufficient detail in [28]. Here, we present new data on the composition of the rock-forming and accessory minerals. The names of the rocks are given according to R.W. Le Maitre [30].

The oldest rocks of the Tommot massif are alkaline pyroxenites represented by jacupirangites. These are dark-green to black, massive, mostly medium-grained rocks. They have a panidiomorphic-granular or sideronitic texture. The average mineral composition of the least modified varieties corresponds to ore jacupirangite. It includes (in %): olivine—4.3, orthopyroxene—1.1, clinopyroxene—59.9, amphibole—14.2, magnetite—13.8, spinel—4.6, nepheline—1.2, melilite—0.8, and apatite—0.1. Up a section, with the appearance of pla-

gioclase, ore jacupirangites get replaced by feldspar jacupirangites with a gabbro-ophitic texture. Their mineral composition varies widely, with averages of (in %): olivine—2.2, orthopyroxene—1.1, clinopyroxene—26.2, amphibole—38.8, biotite—2.1, plagioclase—12.1, magnetite—9.4, apatite—1.2, and spinel—1.3. In both the ore and feldspar jacupirangites, one can observe intergrowths of olivine with orthopyroxene and the substitution of amphibole for pyroxene. Postmagmatic processes with the development of serpentine after olivine, actinolite after amphibole, zeolite after nepheline, and carbonate and albite after plagioclase are widely manifested.

Jacupirangites are cut by numerous subvertical apophyses of alkaline gabbroids up to 2 m thick. Gabbroids of the major body are dominated by dark-gray, massive, medium-grained varieties with an ophitic, hypidiomorphic, or allotriomorphic-granular texture; less common is a corona texture that is due to the development of kelyphitic amphibole rims around pyroxene. In the endocontacts, the rocks have a fine-grained doleritic texture. The average mineral composition of the least modified samples (in %) is: olivine—0.9, pyroxene—7.6, nepheline and melilite—3, amphibole—34.7, biotite—2.1, plagioclase—44.8, K-Na feldspar—0.1, apatite—2.2, magnetite and ilmenite—4.1, titanite and zircon—0.3, and apatite—0.2. The composition varies widely, mainly corresponding to theralite and to a decrease in nepheline content to essexite. Olivine–pyroxene melanocratic rocks predominate in endocontacts, whilst amphibole–pyroxene mesocratic varieties prevail away from the contacts. The gabbroids contain lenses of coarse-grained hornblendites composed of short amphibole prisms and a small amount of plagioclase and magnetite (up to 10% in total). The saturation of hornblendites with coarse-grained apatite (5%–7%) is typical. The gabbroids are pierced with numerous veinlets of coarse-grained pegmatoid syenites.

Syenites are massive coarse-grained rocks, with spots of dark-green minerals against the background of a light-pink feldspar groundmass. They are replaced toward the contacts by fine-grained taxitic varieties. The texture is hypidiomorphic-granular. In leucocratic parts, pyroxene and amphibole fill interstices between feldspar grains, whereas in melanocratic parts, on the contrary, interstices between pyroxene and amphibole are filled with xenomorphic feldspar grains. The mineral composition of the rocks corresponds mainly to alkaline feldspar syenite (in %): mesoperthitic K–Na feldspar—46.5, albite—36.7, kaersutite—9.4, aegirine—0.8, biotite—1.3, magnetite—1.4, titanite—0.7, apatite—0.5, and REE minerals (chevkinite, monazite, allanite)—0.2. Sporadically, there are present relics of single olivine grains. With the growing content of plagioclase, alkaline feldspar syenites grade into foid-bearing monzonites, and with the appearance of a small amount of nepheline (less than 5%), grade into foid-bearing syenites. In foid-bearing monzonites, the amount of plagioclase, which occurs in intergrowths with sanidine and has the composition of 80%–87% *ab*, 10%–13% *an*, and 1%–9% *or*, is up to 5%.

All the rocks of the Tommot massif are strongly broken down, and the primary textures are only fragmentarily preserved. Significant alteration of the rocks makes it difficult to study their mineral composition.

Olivine in the Tommot massif rocks is normally replaced by fibrous serpentine. The $Fe^*/(Fe^* + Mg)$ ratio of the mineral, determined from its rare relics, increases with the SiO_2 content from 23%–31% in jacupirangite, to 38%–53% in alkaline gabbro, to 72% in alkaline syenite. Olivine from jacupirangites contains trace amounts of Ca (0.2% to 0.42%), which is more common for olivine from the rocks of layered intrusions in stable regions. Olivine from gabbroids contains small amounts of Al_2O_3 (0.5%) and Na_2O (0.2%–0.4%), which is typical for olivine of highly alkaline series [31]. The crystallization temperature of olivine from jacupirangites and gabbroids is 1280 and 1120 °C, respectively [32].

Orthopyroxene was only observed in relics, and hence, its chemical composition could not be determined. According to its optical properties, it is identified as the mineral bronzite.

Clinopyroxene, predominant in pyroxenes of the ultrabasic and basic rocks, is represented by magnesian diopside and high-Ca augite (Table S1). The calculated crystallization temperature varies from 1319 °C to 1093 °C at a pressure of 10–13 kbar [33]. Its composition is comparable to that of clinopyroxenes from the rocks of the alkaline series, but some mea-

measurements in the grain cores revealed low $\text{Fe}^*/(\text{Fe}^* + \text{Mg})$ (19%–30%) and TiO_2 (0.3%–0.6%) values corresponding to the composition of pyroxenes from the basic rocks of normally alkaline layered intrusions [31]. The syenites characteristically contain aegirine.

Amphibole first had overgrown pyroxene and then completely replaced it. In the ultrabasic rocks it is represented chiefly by pargasite and kaersutite with calculated crystallization parameters [34,35]: $T = 1071\text{--}1002\text{ }^\circ\text{C}$, $P = 5.7\text{--}7.6\text{ kbar}$, $-\log f_{\text{O}_2} = 9.7\text{--}11.8$, and water content in the melt of 4.3%–7.4% (Table S2). In the basic rocks, along with kaersutite typical of alkaline rocks, there is taramite and magnesiohastingsite present. The crystallization parameters are close to those of amphiboles of the ultrabasic rocks: $T = 1070\text{--}1014\text{ }^\circ\text{C}$, $P = 7\text{--}7.9\text{ kbar}$, $-\log f_{\text{O}_2} = 9.9\text{--}11$, and water content in the melt of 6.3%–6.6%. At shallow-depth conditions, amphibole gets replaced by cannilloite at $T = 820\text{--}829\text{ }^\circ\text{C}$ and $P = 2.6\text{--}3.8\text{ kbar}$. Amphibole is represented in hornblendites by magnesiohastingsite that crystallized at $T = 964\text{--}968\text{ }^\circ\text{C}$, $P = 4.1\text{--}4.4\text{ kbar}$, $-\log f_{\text{O}_2} = 11.8\text{--}11.9$, and water content in the melt of 4.9–5.4%. Amphibole of syenites corresponds to kaersutite that crystallized at $T = 1001\text{--}1037\text{ }^\circ\text{C}$, $P = 4.3\text{--}5.6\text{ kbar}$, $-\log f_{\text{O}_2} = 9.4\text{--}11.6$, and water content in the melt of 6%–6.1%. Ferropargasite was found in relics. The most characteristic compositional feature of amphiboles from the Tommot massif rocks is undersaturation with silica, which is typical for the derivatives of the K-Na alkaline-ultrabasic and alkaline-basic melts.

Biotite from the Tommot massif rocks replaces amphibole or fills interstices between feldspar grains. In gabbroids, it is characterized by $\text{Fe}^*/(\text{Fe}^* + \text{Mg}) = 40.1\%\text{--}59.4\%$ and $\text{Al}/(\text{Al} + \text{Fe}^* + \text{Mg} + \text{Si}) = 19\%\text{--}22\%$, with the crystallization temperatures of $680\text{--}717\text{ }^\circ\text{C}$. In syenites, biotite with $\text{Fe}^*/(\text{Fe}^* + \text{Mg}) = 52.7\%\text{--}53.1\%$, $\text{Al}/(\text{Al} + \text{Fe}^* + \text{Mg} + \text{Si}) = 20.9\%\text{--}21.1\%$, and $T = 670\text{--}722\text{ }^\circ\text{C}$ occurs interstitially in feldspars. At the postmagmatic stage, lepidomelane with $\text{Fe}^*/(\text{Fe}^* + \text{Mg}) = 81.6\%\text{--}83.1\%$, $\text{Al}/(\text{Al} + \text{Fe}^* + \text{Mg} + \text{Si}) = 20.9\%\text{--}21.1\%$, and $T = 670\text{--}673\text{ }^\circ\text{C}$ developed along thin fractures in syenites (Table S3) [36–39].

Plagioclase contains 97%–62% anorthite in the ultrabasic and 75%–52% anorthite in the basic rocks, where the estimated [40] crystallization temperatures are $1132\text{ }^\circ\text{C}$ and $1130\text{--}1087\text{ }^\circ\text{C}$ and the pressures are 13.3–6.8 and 11.2–6.8 kbar, respectively. In syenites, oligoclase–albite, albite (0.2%–5.8% *an*), and sanidine are found, whereas in alkaline syenites, relics of undecomposed K-Na feldspar are present with the close contents of the albite and orthoclase minerals, the calculated crystallization temperature of $1093\text{--}961\text{ }^\circ\text{C}$, and a pressure of 11.2–6.8 kbar.

Magnetite from the ultrabasic and basic rocks is a rock-forming mineral. High-Ti magnetite typical for the alkaline series (up to 10% TiO_2 and up to 5% Al_2O_3 , with a significant admixture of Mg and Na) has been found only in some of the gabbroids.

The main accessory minerals are apatite and zircon. F-OH- apatite is comparable, due to its high Cl content (up to 0.8%) and the Cl/Na ratio = 3–8, to high-temperature apatite of deep-seated magma derivatives [41]. Its REE content does not normally exceed 0.15%, and only in syenites does the Ce concentration reach 0.8%, and that of yttrium 0.3%. Zircon has not been found in the ultrabasic rocks. In gabbroids, zircons are zoned, with the $\text{ZrO}_2/\text{HfO}_2$ ratio varying from 147 to 20. High contents of trace elements (up to 2.5% Y_2O_3 and up to 0.22% Yb_2O_3) are found only in the rims of zircon grains. Syenites are the most rich in zircons ($\text{ZrO}_2/\text{HfO}_2 = 178\text{--}11$). Zircons are stably enriched with Y_2O_3 and ThO_2 , especially those from syenite pegmatites. The content of trace elements increases rapidly towards the periphery of zoned crystals, reaching 1.7% Y_2O_3 and 1.83% ThO_2 . High U values (up to 0.98%) are less common. The ultrabasic rocks contain single grains of chevkinite, bastnaesite, and thorite, whereas in gabbroids and syenites, chevkinite, monazite, and allanite are rarely found.

4.2. Somnitelnyi Massif

The main facies of the Somnitelnyi massif is represented by massive medium-grained alkaline and subalkaline granites grading toward the contact into fine-grained, some-

times porphyritic varieties. The texture is allotriomorphic-granular, but in the contacts a pegmatoid texture also can be observed (Figure 4).

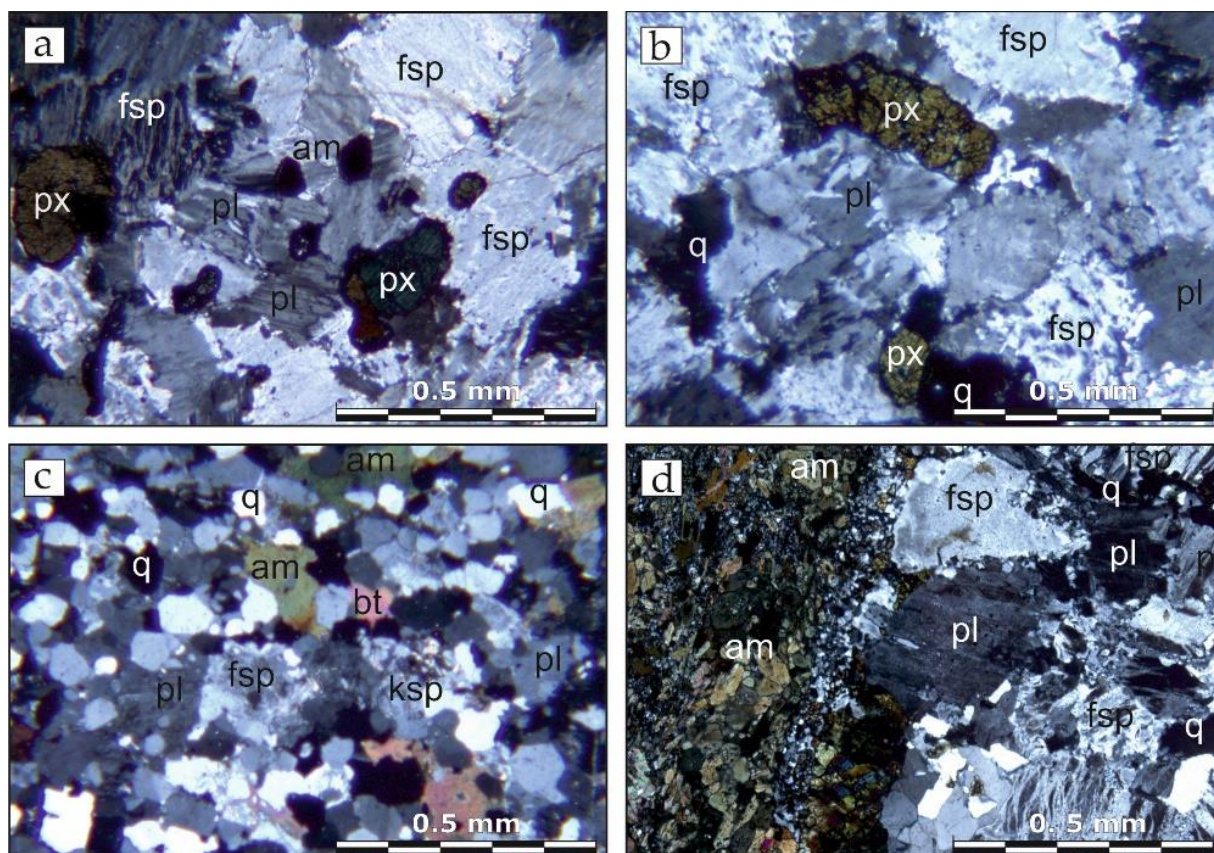


Figure 4. Textures of the Somnitelnyi massif granites. (a,b) Medium-grained granites in the central part of the massif; (c) fine-grained granites in the endocontact of the massif; (d) pegmatoid texture of granites in contact with amphibole–feldspar schists. Crossed nicols. q—quartz, fsp—K-feldspar, pl—plagioclase, am—amphibole, px—pyroxene, bt—biotite.

The granites are composed of mesoperthitic K–Na feldspar; oligoclase–albite or albite, sometimes framed by small prisms of arfvedsonite; and prismatic grains of aegirine–augite and aegirine. The endocontact part is gneissic and has a taxitic-banded texture. The host rocks are intensely fenitized with the development of metasomatic feldspar porphyroblasts and aegirine–arfvedsonite clusters. The exocontact zone is pierced with steeply dipping quartz albite and quartz veins.

The average quantitative-mineralogical composition of the rocks (in %) is: quartz—31.5, plagioclase—22.8, K–Na feldspar—31.9, aegirine–augite and aegirine—8.1, amphibole—2.6, biotite—0.4, ore minerals—2.2, titanite—0.1, and accessory minerals (zircon, apatite, fluorite, allanite, columbite–tantalite, REE minerals)—0.4.

K–Na feldspar shows a diverse internal structure. In the medium-grained rocks in the central part of the Somnitelnyi massif and in porphyritic varieties in endocontacts, mesoperthite with a negative optic axial angle ($2V_{Np} = 20–50^\circ$) prevails. In addition to simple Carlsbad twins, one can observe sectoral intergrowths and the curvature of composition planes with the formation of hourglass-type structures. The optical properties vary widely within each grain. As a result of postmagmatic transformations, domains appeared with a lattice structure and the optic axial angle increased to $70–80^\circ$. The same domains are noted in xenomorphic feldspar grains of the groundmass. The presence of brownish-red hematite is typical, especially for pegmatoid granites, which imparts a dark pink to almost red color to the rocks. The anorthite content is less than 1%, and that of

albite is 3.3%–12.6%. Undecomposed K-Na feldspar with the composition of anorthoclase (47.1% *ab*, 52.7% *or*, 0.2% *an*) and the crystallization temperature of 963–1027 °C [40] was found only in a single sample. Plagioclase either forms slightly elongated plates or it occurs as irregular isometric grains. It contains 0.6%–2% orthoclase, and has a positive optic axial angle ($2V_{Ng} = 50\text{--}90^\circ$). The only determined crystallization temperature is 965–977 °C.

Aegirine-augite is the first of the dark-colored minerals to crystallize. It forms short-prismatic and equant grains, and is crystallized simultaneously with feldspar. The mineral is pleochroic, from grass- or gray-green to brownish-green. Its $Fe^*/(Fe^* + Mg)$ ratio is 53%–63% and the calculated crystallization parameters [33] are: $T = 1011\text{--}1022^\circ\text{C}$ and $P = 8\text{--}10$ kbar (Table S1). Clinopyroxene forms intergrowths with magnetite, titanite, zircon, and xenotime. In one of the aegirine clusters, a relic of fayalite with $Fe^*/(Fe^* + Mg) = 50.3\%$, $CaO = 0.42\%$, and the calculated crystallization temperature of 966–1106 °C was found [32]. Early amphibole occurs as inclusions in plagioclase, and it has a composition of hastingsite with calculated parameters: $T = 937\text{--}943^\circ\text{C}$, $P = 7.1\text{--}7.3$ kbar, and $Fe^*/(Fe^* + Mg) = 63\%\text{--}64\%$ (Table S2). Late magmatic amphibole (arfvedsonite, ferro-eckermannite) prevails, framing aegirine-augite or filling interstices in feldspars. It is pleochroic in shades of blue and green. The mineral is characterized by a negative optic axial angle ($2V_{Np} = 20\text{--}50^\circ$), birefringence ($N_g - N_p = 0.016\text{--}0.020$), and the amounts of $F = 0.49\%\text{--}0.77\%$ and $Cl = 0.02\%\text{--}0.10\%$. The crystallization temperature is 700–801 °C. Postmagmatic aegirine forms large acicular porphyroblasts filled with inclusions of salic minerals of the granites (Figure 5). It is developed mainly in the endocontact zone of the massif and also after the hosting granite gneisses and schists. The $Fe^*/(Fe^* + Mg)$ value is close to 100% (Table S1).

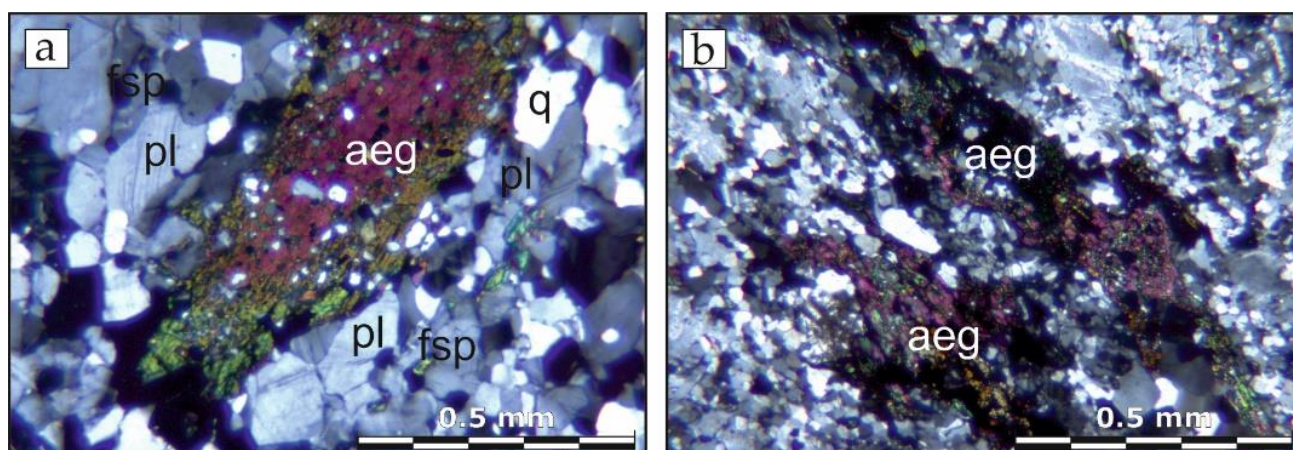


Figure 5. Metasomatic porphyroblasts of aegirine: (a) in granite, (b) in granite gneiss. Crossed nicols. q—quartz, pl—plagioclase, fsp—K-feldspar, aeg—aegirine.

Biotite is not typical for the Somnitelnyi granite massif. Its rare flakes are noted in interstices of salic minerals, where it also forms chains seen along the grain boundaries of these minerals. Less often, large biotite plates with fringed edges and curved cleavage planes are observed. It is pleochroic, from light greenish-brown to dark brown-green to black. Biotite is late-postmagmatic. It crystallized at 641 °C, 0.9 kbar, low ($-\log f O_2 = 14$) oxygen fugacity, and a water content of about 8%. Compositionally, it corresponds to Fe-biotite ($Fe^*/(Fe^* + Mg) = 49.7\%$; $Al/(Al + Fe^* + Mg + Si) = 17.5\%$), which is characteristic of A-type granites, the derivatives of crustal-mantle magmas [42,43] (Table S3).

Of the accessory minerals, zircon with high Y (0.3%–2.34%), Yb (up to 0.8%), U (up to 0.39%), and Th (up to 0.58%) contents is the most characteristic (Table 1). In terms of composition, three groups of zircons are distinguished: magmatic zircons forming inclusions in the rock-forming minerals, with medium Yb and medium-to-low Y contents and $ZrO_2/HfO_2 = 63\text{--}35$; late-postmagmatic zircons in the form of inclusions in quartz and in association with ore minerals, with maximum Y and Yb values and $ZrO_2/HfO_2 = 33\text{--}6$; and the third group with $ZrO_2/HfO_2 = 81\text{--}143$. Zircons of the last group are characterized

by a low Y content and contain no Yb. The first two groups correspond, in terms of their Y_2O_3 – Yb_2O_3 ratios, to zircons from the derivatives of the gabbro–granite series, whereas zircons of the third group lie, in the Yb_2O_3 vs. Y_2O_3 diagram [44], outside the fields of igneous rock zircons (Figure 6). With regard to zircon grain morphology (subrounded and irregular) and the low content of trace elements (Table 1), zircons of the third group are similar to zircons of charnockites or eclogites [45,46]. We interpret zircons of this group to be restitic.

Table 1. Major element contents (wt.%) in zircons of the Somnitélnyi massif rocks.

Sample	Rock	Zone	HfO ₂	ZrO ₂	SiO ₂	ThO ₂	Yb ₂ O ₃	P ₂ O ₅	Y ₂ O ₃	UO ₃	Total	ZrO ₂ /HfO ₂
V28/2-1	granite	center	0.19	65.10	32.83	0	0	0.06	0.16	0	98.34	343
V-28/2-2		center	0.64	65.68	32.51	0.03	0.05	0.10	0.37	0	99.37	103
		middle	0.83	65.84	32.75	0.11	0	0.08	0.32	0	99.94	79
		periphery	1.05	64.74	32.92	0.09	0	0.19	0.51	0	99.49	62
V28/2-3		center	1.01	63.50	36.09	0	0.06	0.05	0.58	0	101.29	63
		middle	1.19	62.02	35.66	0	0.17	0.11	0.75	0	99.90	52
		periphery	1.51	63.19	35.49	0.02	0.05	0.07	0.74	0	101.07	42
		periphery	1.81	62.83	35.67	0	0.07	0.11	0.70	0	101.20	35
V28/2-4		center	1.49	49.67	31.32	0	0.61	0.67	1.00	0	99.75	33
		middle	1.86	49.54	33.28	0	0.61	0.54	1.35	0	100.17	27
		periphery	8.87	56.72	31.73	0.13	0.85	0.61	1.26	0	100.16	6
PR26/7a1	granite	center	1.43	62.12	34.37	0	0	0.10	0.34	0	96.35	43
PR26/7a2		center	2.49	59.51	33.61	0.10	0.27	0.19	0.95	0	97.12	24
		middle	3.51	59.25	33.60	0.11	0.04	0.18	0.55	0	97.23	17
		middle	3.63	59.17	33.87	0.02	0.12	0.10	0.39	0	97.30	16
		periphery	4.63	58.91	33.78	0	0.08	0.24	0.74	0	98.38	13
2313/1		center	2.26	66.60	30.28	0.01	0	0.13	0.31	0	99.59	29
		middle	2.57	63.11	31.35	0.15	0.13	0.21	0.92	0	98.43	25
		periphery	2.98	62.24	30.36	0.16	0.17	0.30	1.07	0	97.28	21
Pr24/4a	albitite	center	2.84	61.18	32.67	0.04	0.21	0.22	0.69	0	97.86	22
		middle	3.50	59.79	33.45	0	0.14	0.08	0.46	0	97.41	17
		periphery	6.06	58.62	32.73	0.12	0	0.11	0.60	0	98.24	9.7
PRT14/3	albitite	center	5.49	60.92	32.72	0	0.25	0.28	0.34	0	100.01	11
		middle	6.04	61.06	32.86	0	0.25	0.25	0.45	0	100.91	10
		periphery	7.46	57.79	33.10	0	0.03	0.25	0.62	0	99.25	8
PRT14/3	albitite	center	1.63	63.09	32.68	0.16	0.27	0.27	1.12	0	99.22	39
		middle	4.21	58.25	32.69	0.09	0.34	0.41	1.23	0.02	97.25	14
		periphery	6.59	58.65	33.43	0	0.08	0.25	0.78	0	99.78	9
PR1/2b-1	pegmatite	center	17.00	49.38	1.72	0.09	0.36	0.40	1.24	0	100.20	3
		middle	11.04	55.66	31.38	0.07	0.72	0.71	1.15	0	100.74	5
		middle	14.60	51.34	32.17	0.03	0.41	0.53	1.08	0	100.15	3.5
		periphery	20.27	48.16	31.57	0	0.19	0.30	0.92	0	101.41	2.4

Table 1. Cont.

Sample	Rock	Zone	HfO ₂	ZrO ₂	SiO ₂	ThO ₂	Yb ₂ O ₃	P ₂ O ₅	Y ₂ O ₃	UO ₃	Total	ZrO ₂ /HfO ₂
PR1/2b-2	pegmatite	center	16.31	47.16	32.84	0.02	0.38	0.69	1.50	0	98.91	2.9
		middle	16.68	48.80	32.64	0.06	0.22	0.62	1.36	0	100.36	2.9
		periphery	18.48	45.90	33.36	0	0.23	0.45	0.90	0	99.31	2.5
PR1/2b-3	pegmatite	center	11.64	53.39	32.61	0.10	0.46	0.74	1.17	0	100.09	4.6
		middle	34.15	32.94	31.40	0.05	0.05	0.29	1.12	0.35	100.36	1.1
		middle	35.84	33.14	30.35	0.06	0.16	0.53	1.42	0.3	101.90	0.9
		periphery	33.13	35.71	31.18	0.10	0.10	0.29	1.12	0	101.64	1.1

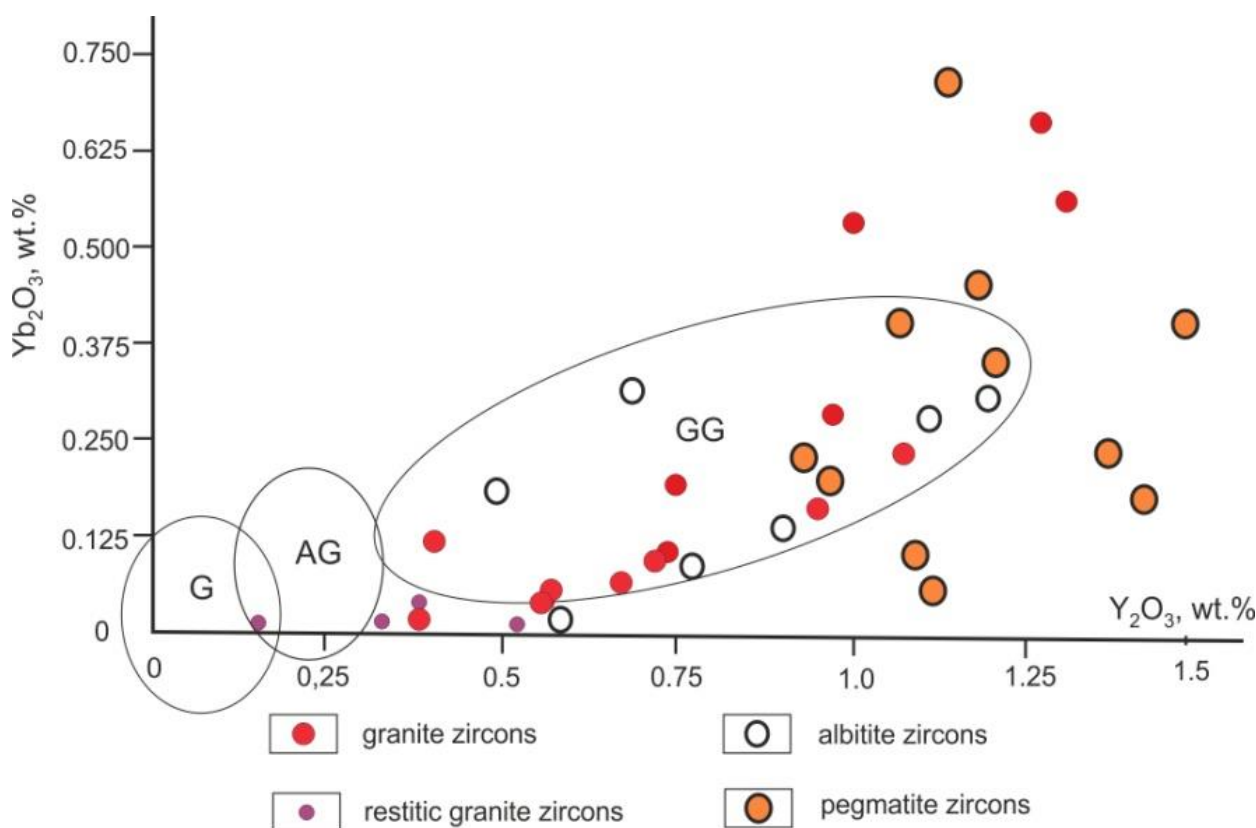


Figure 6. Yb₂O₃ vs. Y₂O₃ diagram for zircons from the rocks of the Tømmot ore field. Fields in the diagram [44]: G—granite–leucogranite, AG—adamellite–granite, GG—gabbro–granite associations.

Other accessories include columbite–tantalite and REE minerals (chevkinite, monazite, allanite). The maximum number of accessory minerals is found in the contact zone, where both the granites and the host rocks are highly saturated with acicular apatite (F–OH apatite with a total amount of Ce₂O₃ and Y₂O₃ up to 1.5% and Sr content up to 0.59%) and nests of fine-grained fluorite and ore minerals, and contain clusters (1–2 cm) and veinlets of REE minerals. Magnetite with low TiO₂ and SiO₂ (up to 1.6%) and manganous ilmenite (3.26%–7.1% MnO) are also common.

The quartz albitite veins are localized mainly in granite gneisses and schists close to being in contact with the granites. The rocks are massive, fine-grained, with a xenomorphic-granular and, less common, granoblastic structure. Their composition is dominated by isometric albite grains (1%–8% *an*, 2V_{N_g} = 59–70°) that are untwinned or have cross-blocked albite twins. Less frequent are grains of sanidine or high orthoclase (2V_{N_p} = 20–40°) and equant rounded quartz grains. In this fine-grained groundmass are set skeletal grains of aegirine, blue-green arfvedsonite, or ferro-eckermannite (pleochroic from dark-blue to

yellowish-green, Np: $c = 0^\circ$, $2V_{Ng} = 80^\circ$, $f = 84\%–99\%$). Amphibole is characterized by varying concentrations of halogens ($F = 0.15\%–1.69\%$, $Cl = 0.01\%–0.66\%$). It forms intergrowths with topaz grains and is often saturated with finely disseminated REE mineralization. Amphibole clusters are fringed and cut by veinlets of highly pleochroic reddish-brown chevkinite in association with large idiomorphic grains of zoned zircon enriched in Hf ($ZrO_2/HfO_2 = 2–3$, in some cases no more than 0.9) (Table 1, Figure 7). It has the maximum Y contents determined for zircons from magmatic rocks of the Tommot ore field (up to 2.3%). Besides, it is higher in U (up to 0.39%) and Th (up to 0.22%) than zircons from the granites. Other accessory minerals include high-Mn (7.8%–17.3% MnO) ilmenite and late-magmatic apatite with low Cl (0.1%–0.36%) and F varying from 2.2 to 4.1%.

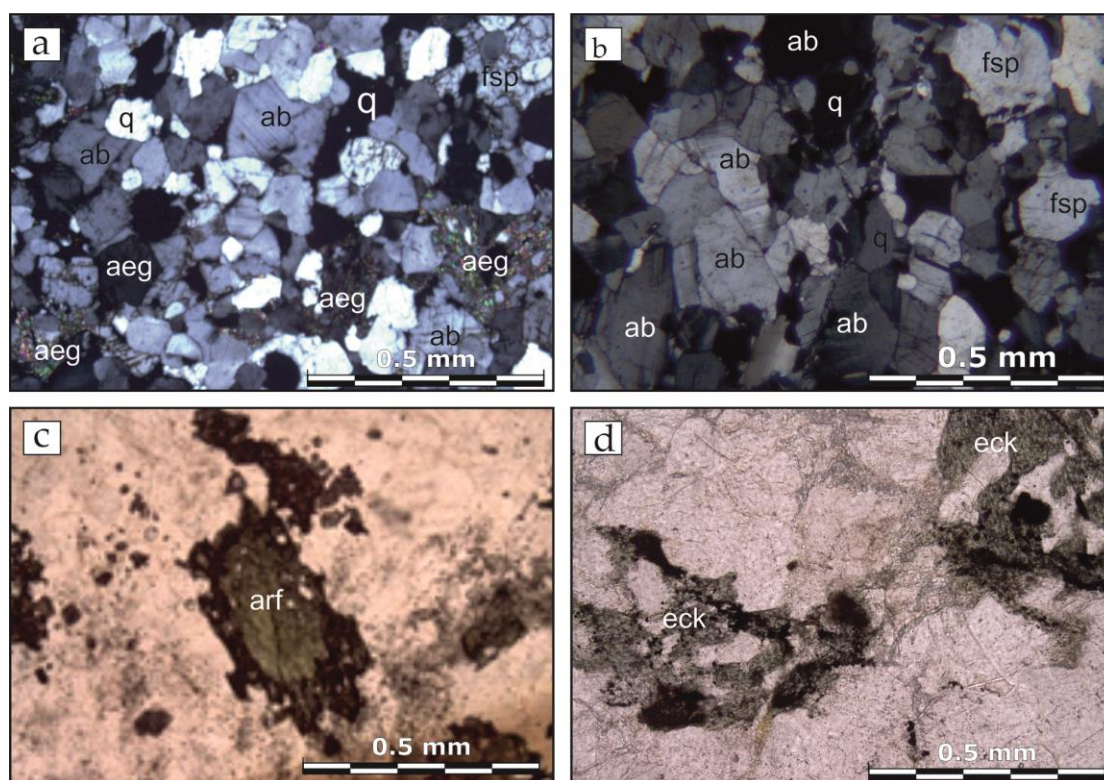


Figure 7. Petrography of quartz albitites. (a) Fine-grained, (b) medium-grained. Crossed nicols. (c) Arfvedsonite fringed by chevkinite in albitite. Parallel nicols. (d) Ferro-eckermannite clusters with nests of REE minerals in albitite. Parallel nicols. q—quartz, ab—albite, aeg—aegirine, arf—arfvedsonite, fsp—K-feldspar, eck—ferro-eckermannite.

Bodies of albite–quartz–feldspar metasomatites composed of microcline–perthite (45%–70%), albite (0%–25%), quartz (10%–20%), aegirine (10%–25%), ferro-eckermannite (up to 10%), and accessory fluorite, zircon, and chevkinite (1%–10%) are much less common.

The granites and the host rocks are intensely broken down and fenitized along the contact. The main ore body is composed of thin-banded rocks of a quartz–feldspathic composition, among which there occurs veins and veinlets of quartz and fine-grained quartz albitites. In quartz veins, ore minerals are confined to clusters of amphibole of the arfvedsonite series, whereas in albitites they fringe and cut such amphiboles. In thin-banded ores, the alkaline amphiboles and ore mineralization are localized along foliation. Along thin fractures in the rocks, veinlets of hematite, fluorite, carbonate, and, less often, chlorite and epidote are developed. In total, 16 REE minerals have been found. The composition of REE mineralization is dominated by chevkinite and yttrialite (Table 2).

Table 2. Composition of main ore minerals of the Tommot deposit (in wt.%).

Mineral	La ₂ O ₃	Ce ₂ O ₃	Nd ₂ O ₃	Eu ₂ O ₃	Y ₂ O ₃	Nb ₂ O ₅	UO ₂	ThO ₂	TiO ₂	SiO ₂	Al ₂ O ₃	CaO	Fe ₂ O ₃	P ₂ O ₅	Total
britholite *	3.49	13.9	11.52	1.22	9.52	0.16	0.28	0.69	0.08	19.35	0.21	9.74	0.73	3.12	74.01
britholite *	3.87	16.07	12.13	1.35	9.4	0.28	0.31	0.92	0.06	19.93	0.19	10.74	0.76	3.77	79.77
gadolinite	0.62	3.66	1.93	0.38	28.72	0.29	0.18	0.55	0.12	23.49	0.31	1.18	8.81	0.14	70.38
gadolinite	0.87	4.84	2.93	0.54	28.98	0.41	0.21	0.7	0.17	23.75	0.32	1.15	9.43	0.18	74.47
yttrialite *	0.78	3.87	2.43	0.5	22.93	0.39	0.45	17.92	0.17	27.25	3.83	0.5	0.82	0.21	82.05
yttrialite *	1.03	3.81	1.7	0.45	24.56	0.43	0.52	20.68	0.22	29.32	2.41	0.55	0.62	0.23	86.53
monazite	16.27	30.82	12.11	0.71	0.41	0.07	0.16	5.16	0.15	2.15	0.35	0.15	0.1	29.93	98.54
monazite	17.84	31.5	11.8	1	1.03	0.34	0.45	4.43	0.18	2.06	0.36	0.11	0.11	30.32	101.27
allanite	4.09	10.76	4.87	0.41	0.54	0.08	0.12	0.47	2.31	30.49	11.28	13.23	16.61	0.04	95.3
allanite	8.47	11.01	3.27	0.25	0.12	0.06	0.1	0.56	1.57	33.51	13.38	11.06	16.04	0.03	99.43
titanite	0.2	1.58	1.59	0.22	3.11	1.22	0.03	0.23	34.01	28.77	1.46	20.31	1.83	0.22	94.78
titanite	0.14	1.31	0.99	0.24	3.4	0.97	0.03	0.44	33.61	28.51	2.05	22.15	2.26	0.13	96.25
thorite	0.14	0.32	0.17	0.09	0.52	0.14	2.14	74.11	0.03	16.96	0.53	1.15	0.35	0.49	97.14
thorite	0.21	0.86	0.07	0.07	0.54	0.67	2.75	72.79	0.03	16.7	0.48	0.92	0.95	0.84	97.88
fergusonite *	0.24	6.6	0.46	0.34	12.73	36.29	0.51	4.32	6.1	3.01	0.64	0.36	11.15	0.17	82.38
aeschynite (Nd) *	0.51	4.37	1.72	0.15	0.62	58.91	4.52	1.52	5.37	0.91	0.08	11.06	0.08	0.06	89.88
aeschynite (Nd) *	0.98	4.88	2.16	0.04	0.49	62.39	4.35	1.28	4.97	0.61	0	10.83	1.05	0.01	92.94
aeschynite (Nd) *	1.55	5.9	2.44	0.24	0.9	55.05	2.55	0.68	6.27	2.47	0.75	13.29	2.84	0.27	95.21
chevkinite	9.99	23.59	9.58	0.74	0.78	0.86	0.14	0.97	17.62	19.9	0.49	0.74	10.16	0.1	95.66
chevkinite	10.61	25.04	10.01	0.83	0.73	0.88	0.14	71	18.41	20.56	0.52	0.71	10.4	0.16	99.71

Notes: *—hydroxyl-containing metamict and hydrolyzed minerals. The contents of HREE were not determined.

The following ore mineral types have been identified at the deposit: monazite–chevkinite with yttrium–fluorite, britholite, and priorite; titanite–britholite with yttrium–carbonate and yttrium–fluorite; fergusonite–chevkinite–britholite with REE borosilicates; and columbite–pyrochlore–xenotime–cyrtolite disseminated ores in albitized aegirine granites. In view of this mineralogy, these are complex ores for Ce–Y mineralization.

5. Geochemistry of Magmatic Rocks

The chemical composition of the Tommot massif rocks varies from ultrabasic to silicic. Alkaline rocks prevail, subalkaline varieties are less common, and those of normal alkalinity are very rare (Table S4, Figure 8) [47–50]. In the diagram for the petrochemical series, the data points of the rocks are localized between the evolution trends of the alkaline-basaltic and basanitic series (Figure 9) [51,52].

The first phase of the Tommot massif is represented by foidites and alkaline gabbroids. The rocks are magnesian and magnesian-ferruginous ($\text{FeO}^*/(\text{FeO}^* + \text{MgO}) = 0.45\text{--}0.76$, avg. 0.61). They belong mainly to the K–Na series, with deviations to the shoshonitic and Na-alkaline series ($\text{Na}/\text{K} = 1\text{--}7$, avg. 3.2). They have low to medium alumina content ($\text{Al}_2\text{O}_3/(\text{FeO}^* + \text{MgO}) = 0.32\text{--}1.22$, avg. 0.77). The rocks are nepheline-normative, and 50% of samples are also leucite-normative. The differentiation index ($\text{DI} = \text{q} + \text{ab} + \text{or} + \text{c}$ normative [53]) is from 3.9% to 29%. The minimum DI is noted for the rocks at the lower horizons of platy bodies, increasing up the section from 31.5% to 43% with the SiO_2 content. The rocks are enriched with F (up to 0.28%, avg. 0.11%) and Cl (up to 0.27%, avg. 0.10%) (Table S4). The parent melt was generated at $T = 1300\text{--}1400\text{ }^\circ\text{C}$ [47] and $P = 35\text{--}40\text{ kbar}$ [49].

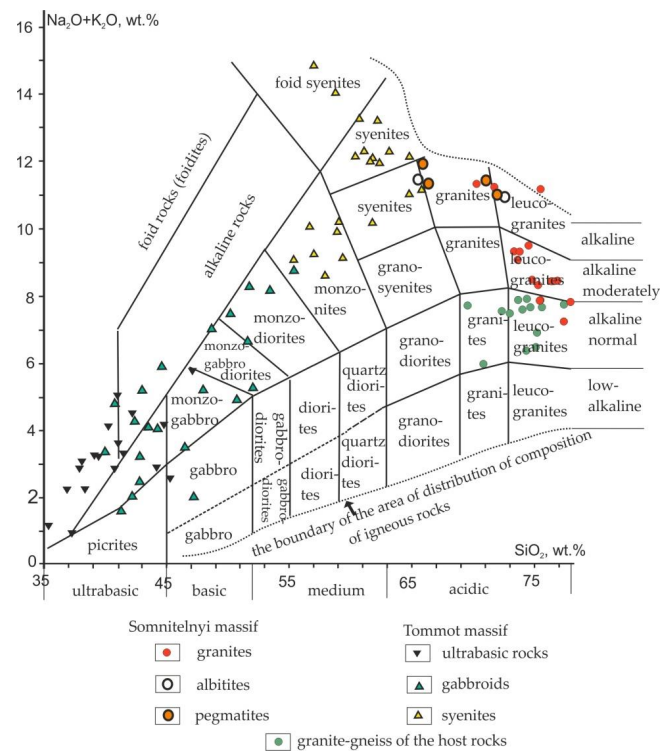


Figure 8. TAS diagram for rocks of the Tommot ore field. Diagram fields after [50].

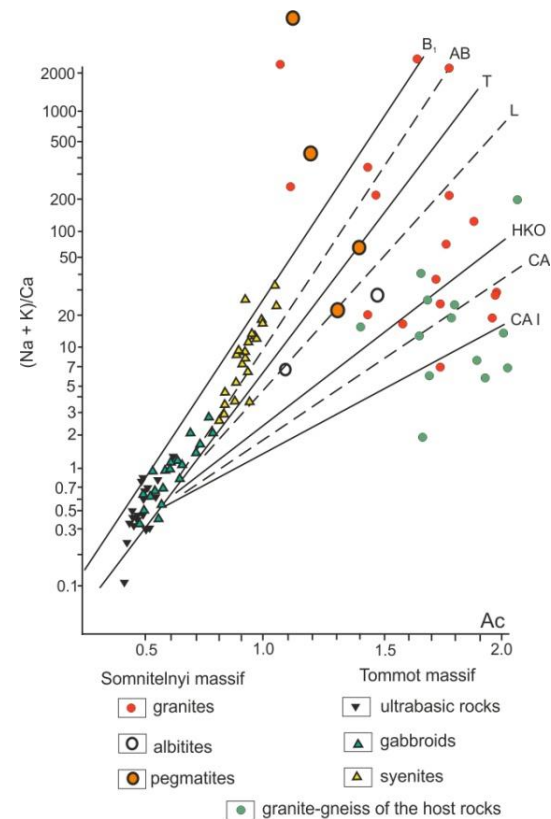


Figure 9. $(\text{Na} + \text{K})/\text{Ca}$ vs. Ac diagram for rocks of the Tommot ore field. Symbols [51,52]: Ac —cation activity ($\text{Ac} = 4\text{Si}/\Sigma(\text{Me} \times \text{Bc})$, where Me = amount of cations of rock-forming oxides $\times 1000$; Bc —basicity of cations; $\Sigma(\text{Me} \times \text{Bc})$ —sum of $(\text{Me} \times \text{Bc})$ for each major oxide except for SiO_2 [51,52]; evolution trends: CAI—calc-low-alkaline (island-arc); CA—calc-alkaline (collision); HKO—high-potassium (orogenic), L—latitic; T—trachytic; AB—alkaline-basaltic; B_1 —basanitic.

The composition of the second phase varies from alkaline-ultrabasic rocks to monzodiorites, with a predominance of monzogabbro and monzogabbro-diorites. They have varying Fe and Al values ($\text{FeO}^*/(\text{FeO}^* + \text{MgO}) = 0.45\text{--}0.9$, avg. 0.71; $\text{Al}_2\text{O}_3/(\text{FeO}^* + \text{MgO}) = 0.41\text{--}2.55$, avg. 1.3) higher than those for the first-phase rocks. They belong to the K-Na alkaline series, with deviation to the Na-alkaline one. With rare exceptions, the rocks are nepheline-normative. Normative leucite was found only in 10% of samples. The DI is higher than for the rocks of the first phase, being up to 52%, with a tendency to increase up the section. As with the rocks of the first phase, enrichment with volatiles is observed here: up to 0.25% F and up to 0.20% Cl (avg. 0.10% and 0.14%, respectively). The parent melt was generated at $T = 1200\text{ }^\circ\text{C}$ [47] and $P = 20\text{--}25\text{ kbar}$ [49].

The composition of the third-phase rocks varies from monzonites and alkaline syenites (in dykes) to foid syenites. The differentiation index (DI) for syenites varies from 63 to 88%. The rocks belong to the K-Na alkaline series, and have high $\text{FeO}^*/(\text{FeO}^* + \text{MgO}) = 0.74\text{--}1$ (average 0.91) and $\text{Al}_2\text{O}_3/(\text{FeO}^* + \text{MgO}) = 1.63\text{--}18.8$ (average 5.3). Nepheline-normative compositions prevail, whereas quartz-normative compositions (up to 12.8% q) are less common. The F and Cl contents are slightly lower than in the rocks of the first and second phases (average 0.07% and 0.09%, respectively). Parameters of the parent melt generation are: $T = 900\text{--}1000\text{ }^\circ\text{C}$, $P = 15\text{--}17\text{ kbar}$.

The compositions of the Somnitenlyi massif rocks range from normally alkaline, to moderately alkaline, to alkaline granites and leucogranites (Table S5) [54,55]. In the diagram by A. Streckeisen and P.W. Le Maitre [56], their data points deviate from the field of alkaline feldspar granites toward the fields of syenogranites and quartz alkaline feldspar syenites (Figure 10).

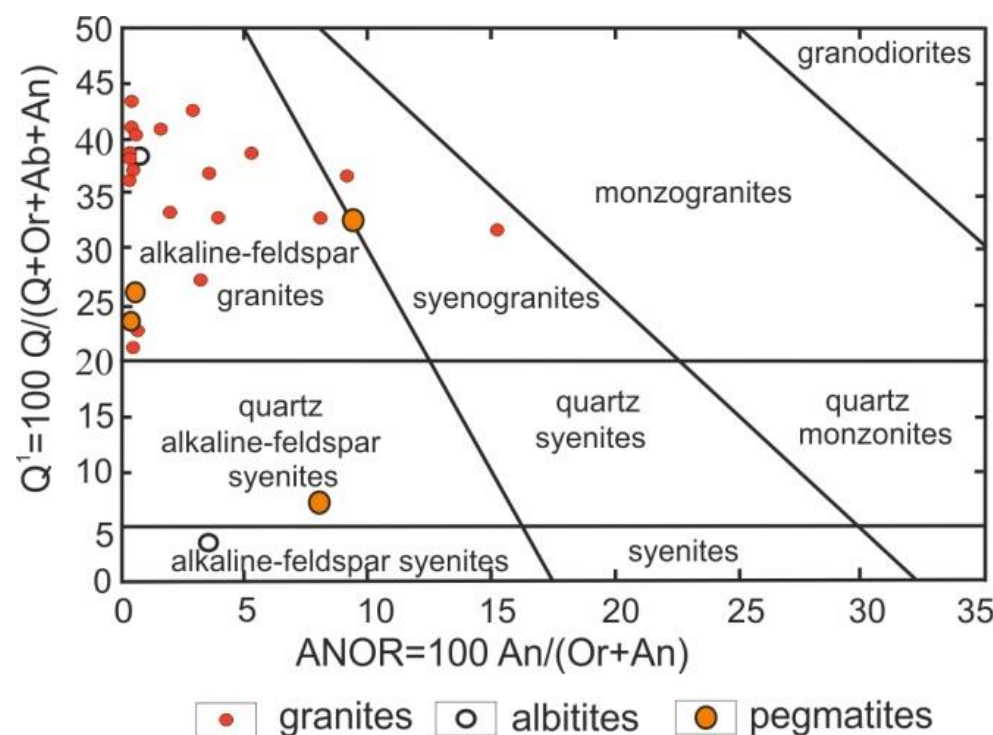


Figure 10. Classification diagram (after [56]) for rocks of the Somnitenlyi massif and Tommot deposit.

Despite the widely manifested metasomatic alteration processes (albitization of feldspars, development of secondary amphiboles) in the granites of the Somnitenlyi massif, it is possible to distinguish general features in the composition of all its rocks. In the above discrimination diagrams, their data points define a trend independent of the main evolutionary trends, as is typical for A-type granites (Figures 8 and 9). At the same time, they differ clearly from the host granite gneisses, having a composition corresponding to that of granites and leucogranites

of normal alkalinity and showing a wide scatter in the lower part of the diagram for the petrochemical series (Figure 9).

The granites are quartz-normative, and about half of them are hypersthene- and/or acmite-normative. The normative corundum was only determined in four samples in an amount of up to 2.7%. The amounts of normative *ab* and normative *or* vary widely due to frequent, intense albitization of the rocks, but their average contents are close (31.6% and 27.2%, respectively). The differentiation index for the granites is from 78.5% to 95.3%, with an average of 89.6%. Of note is low H₂O (0.03%–1.01%, avg. 0.34%) and high Cl (0.14%–0.15%), with F varying within 0.02%–0.22% (average 0.10%). The rocks are low to moderately aluminous (index of Shand Al/(Na + K + Ca) mol. = 0.7–1.2) and highly ferruginous (FeO*/(FeO* + MgO) = 89%–99%). These values, along with the ratios between major petrogenic oxides and the Sr–Rb/Sr ratio, indicate they belong to postorogenic or rift-related A-type granites (Figures 11–15) [57–61]. The maximum calculated temperature of the melt [54] is 1045 °C, the pressure in the magma generation area is up to 9.5 kbar [55], and the crystallization temperature is estimated to be within 1030–746 °C (zircon and apatite saturation temperatures) [21]. According to all of their composition parameters, the rocks are ascribed to A-type postorogenic granites.

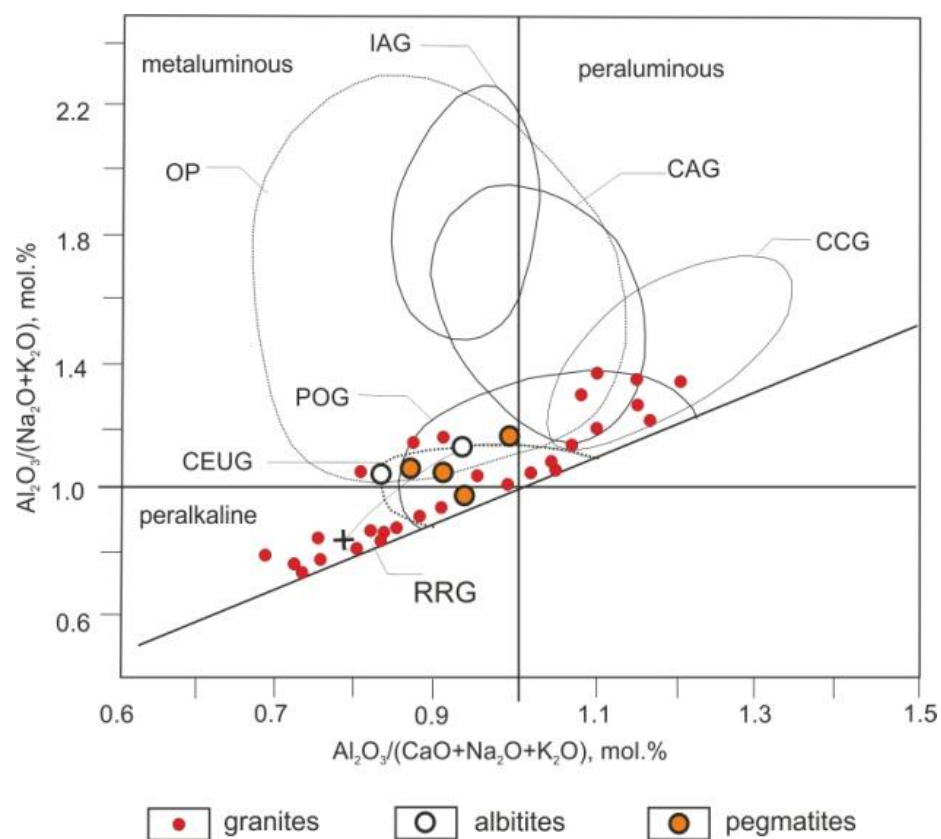


Figure 11. $\text{Al}_2\text{O}_3/(\text{Na}_2\text{O} + \text{K}_2\text{O})$ vs. $\text{Al}_2\text{O}_3/(\text{CaO} + \text{Na}_2\text{O} + \text{K}_2\text{O})$ diagram for rocks of the Somnitselny massif and Tommot deposit [57]. Fields include: IAG— island arcs; CAG—continental arcs; CCG—continental collision settings; POG—postorogenic; CEUG—continental epirogenic uplifts; and RRG—rift-related.

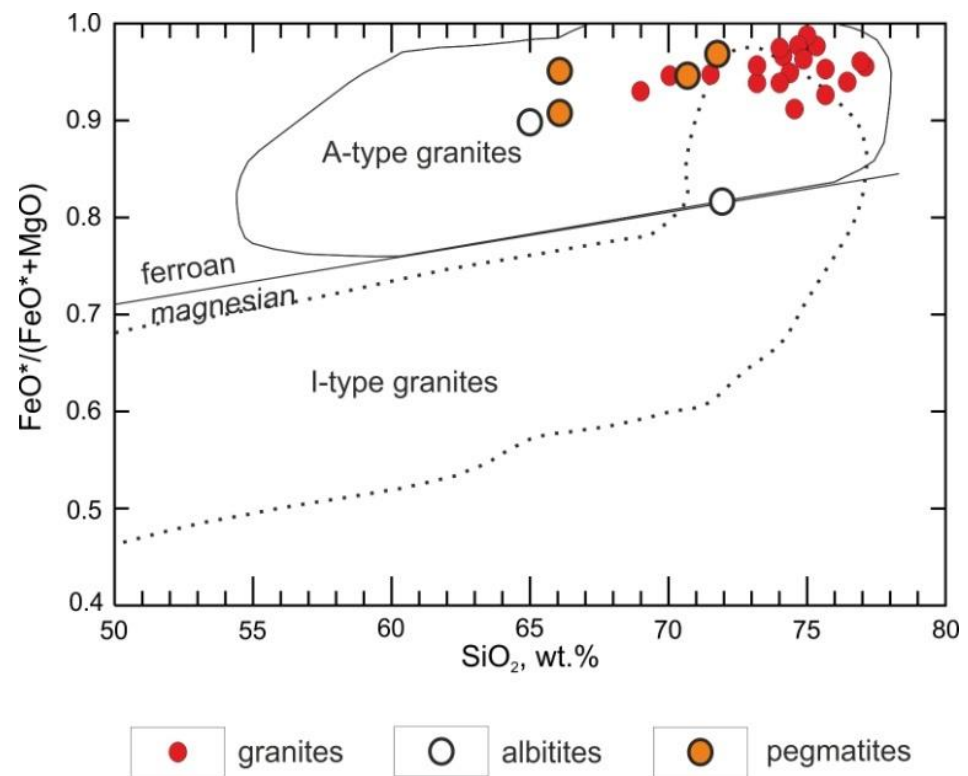


Figure 12. $\text{FeO}^*/(\text{FeO}^* + \text{MgO})$ vs. SiO_2 diagram [58] for rocks of the Somnitelnyi massif and Tommot deposit.

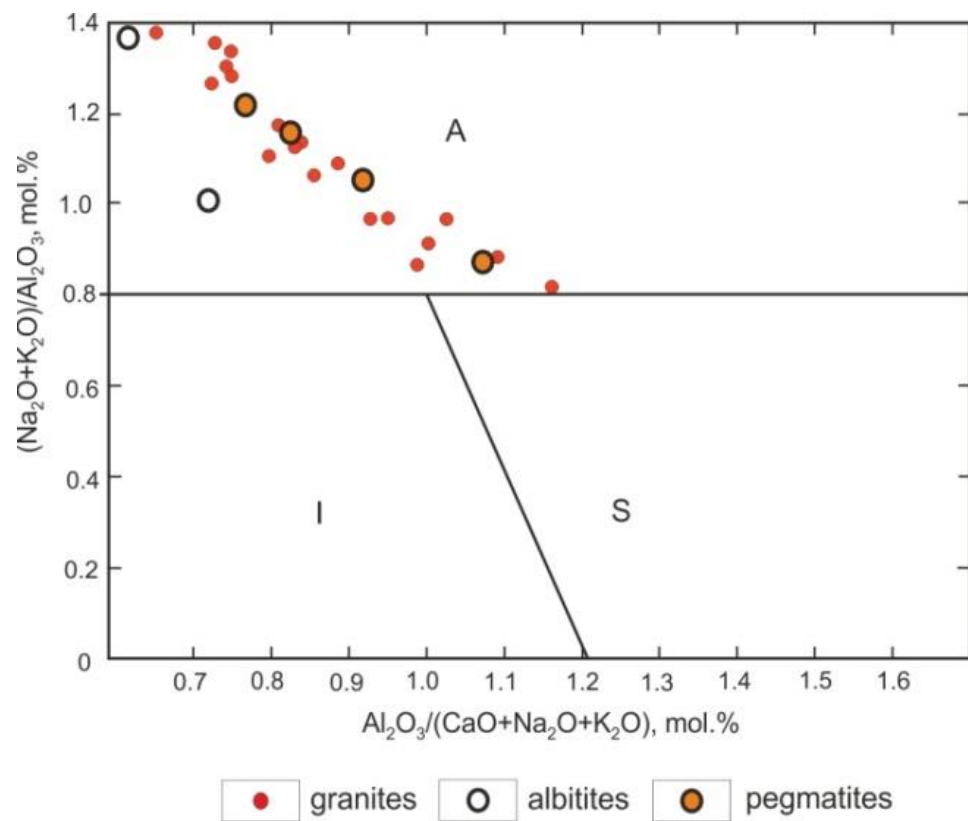


Figure 13. $(\text{Na}_2\text{O} + \text{K}_2\text{O})/\text{Al}_2\text{O}_3$ vs. $\text{Al}_2\text{O}_3/(\text{CaO} + \text{Na}_2\text{O} + \text{K}_2\text{O})$ diagram for rocks of the Somnitelnyi massif and Tommot deposit. Fields on the diagram are from [59]. I, S, A—petrographic types of granitoids.

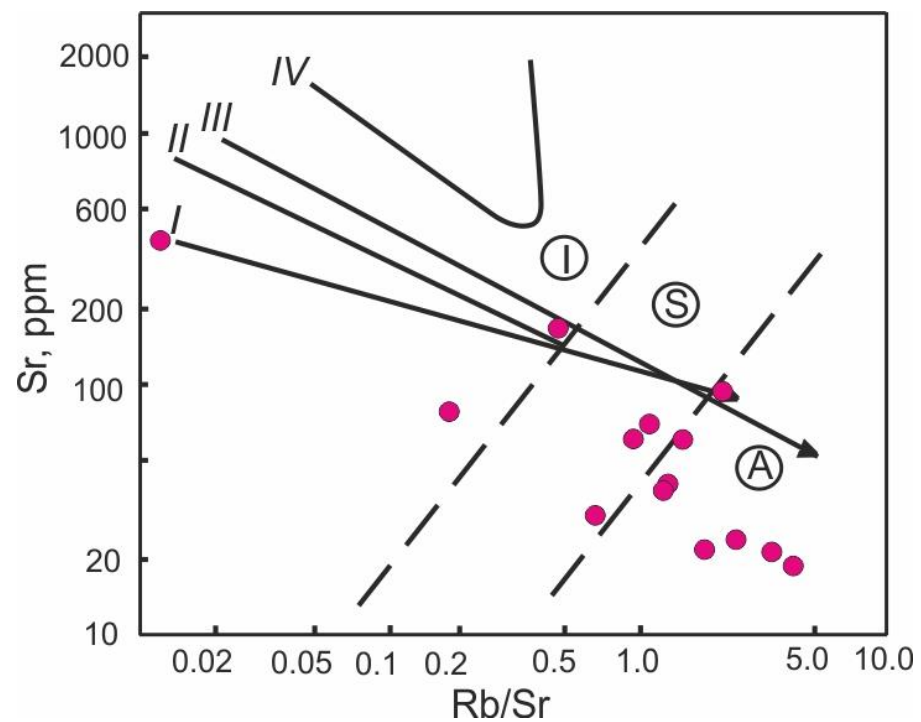


Figure 14. Sr vs. Rb/Sr diagram for granites of the Somnitelnyi massif. Differentiation trends for granitic series [60]: I— island-arc tholeiitic; II— island-arc calc-alkaline; III— active margin calc-alkaline; IV— continental rift zones; and I, S, A— petrographic types of granitoids.

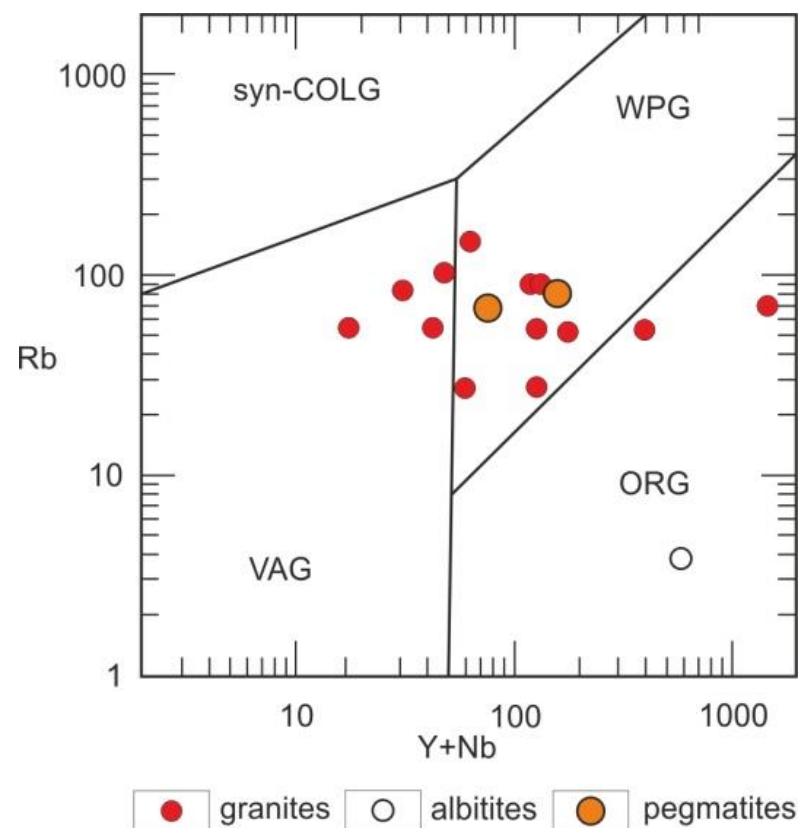


Figure 15. Rb vs. (Y + Nb) diagram for rocks of the Somnitelnyi massif and Tommot deposit. Fields of granitoids: VAG— volcanic arcs, ORG— oceanic ridges, WPG— within-plate, syn-COLG— syncollisional [61].

The host granite gneisses do not contain normative acmite, and 60% of samples contain normative corundum (up to 5.2%, avg. 1.2%). The content of the albite mineral is slightly higher than that of the orthoclase mineral (on average, 32.1% and 25.2%). In terms of SiO₂-K₂O ratios, they correspond to continental granophyres less often to continental trondhjemites [62].

The chemical composition of albitites and pegmatites is variable since they were subject to intensive metasomatic processes. The formation of ferro-eckermannite resulted in the lower silica content, and the development of microcline led to higher K amounts. Therefore, Table S5 and the diagrams (Figures 8–13) show only two of the most representative analyses of albitites and four analyses of pegmatites. The least altered albitite is characterized by a marked predominance of albite over orthoclase in the normative composition (60.1% and 23.4%). The normative composition of pegmatites is featured by widely varying quartz, albite, and orthoclase. However, such as the granites of the massif, these are acmite-bearing rocks (up to 11%) with no normative corundum.

As compared to the Clarke values, the ultrabasic rocks of the Tømmot massif are enriched in Li, Rb, Sr, V, Ce, Sm, Yb, Hf, and Zr and depleted of Cr, Ni, and Co [62]. Only Ba, Sr, and Nb concentrations in gabbroids noticeably exceed the Clarke concentrations, with a deficiency in Cr, Ni, and Co. Syenites, on the contrary, are enriched with Cr, Ni, Co, and Nb relative to the Clarke values. However, in general, Rb, Ba, Sr, Zr, Nb, La, Ce, Gd, Tb, and Lu contents increase from ultrabasic rocks to syenites, whereas the amounts of Cr, Ni, V, and Co decline (Table 3). The rest of the elements have sub-Clarke values that were preserved during the evolution process.

Table 3. Average contents of trace elements (ppm) in magmatic rocks of the Tømmot and Somnitelny massifs [27] and Clarke values [63].

	Tommot			Somnitelnyi		Clarke, ppm		
Elements	Ultrabasic Rocks	Gabbroids	Syenites	Granites	Ultrabasic Rocks	Gabbroids	Syenites	Granites
Cl, %	400	400	600	1000	74	80	470	190
F, %	1000	1400	1000	1500	100	400	1200	820
Li	11	19	10	16	0.75	15	28	37
Rb	18	26	52	13	0.7	37	110	180
Ba	482	628	963	200	0.8	290	1600	750
Sr	863	1372	1620	70	7	460	200	150
Cr	58	34	26	24	2000	1800	2	5.6
Ni	75	32	12	10	200	140	4	3.5
V	315	192	33	13	42	240	30	38
Co	63	40	7	2	150	48	3	1
Zr	120	180	569	420	43	130	500	180
Nb	20	68	147	260	13	19	35	21
La	6.5	15.5	65	223	3.9	17	45	48
Ce	56	80	95	163	8.6	48	95	72
Sm	5.2	10	9	6	0.83	5.3	10	7.5
Eu	2	2.2	1.9	1	0.24	1.3	1.8	1.4
Gd	1	2	3.5	5.6	0.93	5.2	10	6.8
Y	28	32	27	55	2	23	17	50
Yb	3.4	3.3	3	4	0.48	2	4.3	4
Tb	0.5	1	1.5	1.6	0.2	0.83	1.6	1.1
Lu	0.2	0.3	16	1.7	0.068	0.5	1.2	0.9
Hf	7	9.9)	13	30	0.46	2.6	11	3.9

The subalkaline and alkaline granites of the Somnitelny massif are enriched with Cr, Ni, V, Zr, Nb, La, Ce, and Hf and depleted of Li, Rb, Ba, and Sr (Table 3). In terms of REE, Zr, Nb, and Hf values, they are intermediate between rare-metal granites of the alkaline series, presumably of palaeogenetic origin, and agpaitic alkaline granites, which are the late derivatives of alkaline-basaltoid magmas [62,64]. Their Li, Rb, Zr, Cr, Ni, and V

contents are identical to those in crustal palingenetic granites of the alkaline series, and the concentrations of Ba, Sr, Sn, and Zn are intermediate between rare-metal granites of the alkaline series and crustal palingenetic granites of the alkaline series. In the Ba–Rb–Sr diagram [65], their data points plot mainly into the field of alkaline rare-metal granites (Figure 16).

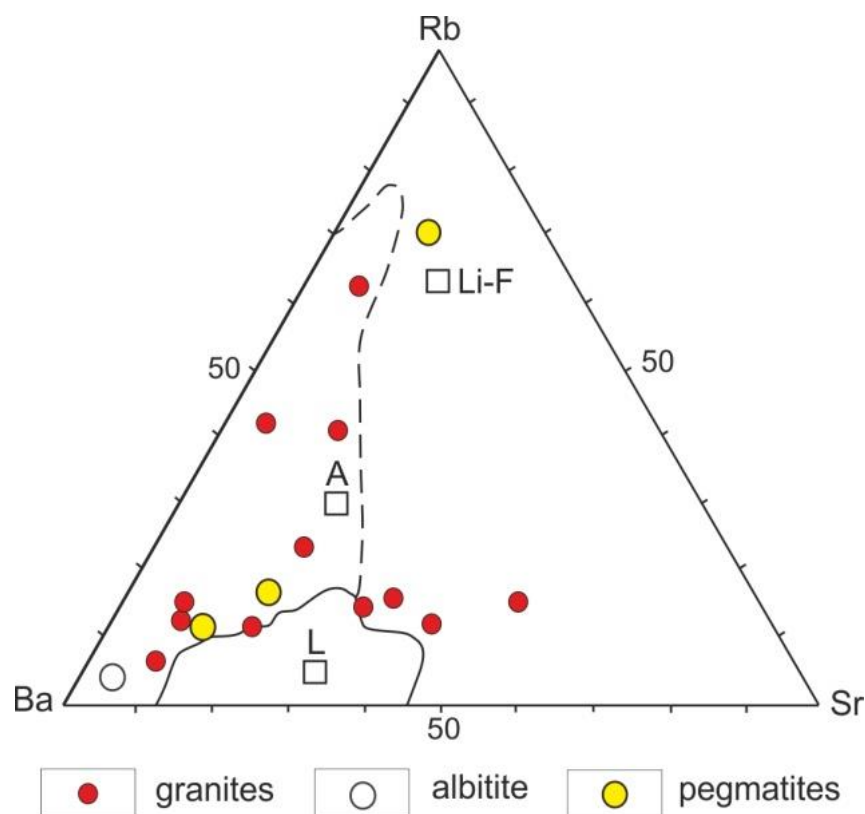


Figure 16. Ba–Rb–Sr diagram for rocks of the Somnitelnyi massif and Tommot deposit. Fields in the diagram [65]: A—rare-metal alkaline granites, L—latitic granites, Li-F—plumasitic lithium-fluoride granites.

Table 4 presents the results of determining REE contents in the rocks of the Tommot ore field obtained by ICP–MS analysis, and Figure 17 shows their distribution trends. La, Sm, and Gd contents in the least modified granites of the Somnitelnyi massif are 2–3 times higher than the Clarke values for the granites, with other REEs present at sub-Clarke levels. However, the total REE content in the granites is an order of magnitude higher than in the host schists. In the course of metasomatic fenitization, concentrations of Ce- and Y-group elements increased rapidly, reaching a maximum in pegmatites and fenites.

Table 4. REE and rare-metal contents in the rocks of the Tommot ore field (in ppm).

Sample	FT 4/5	PT 7/1	TR 117/1	TR 114/2	PR 8/1	P 2313/2	O 24/3	PR 14/1	K 106	P 2350/3	O 26/2	R 2351/1	PR 90/1	O 24/2a	PR 26/2
rock	granite				albitite				pegmatite		schists		fenitized granite gneiss		
La	90	180	160	130	180	530	60	1700	280	1400	46	8.5	80	430	320
Ce	64	120	70	100	120	270	70	700	140	650	120	14	56	320	170
Pr	6	14	7	7.5	9	25	5.5	60	10	40	4.8	1.3	3.8	42	14
Nd	28	55	27	26	33	100	30	230	40	170	16	4.2	18	150	63
Sm	10	25	7.5	8.5	10	15	17	25	16	30	5.5	1.5	8.5	45	20

Table 4. Cont.

Sample	FT 4/5	PT 7/1	TR 117/1	TR 114/2	PR 8/1	P 2313/2	O 24/3	PR 14/1	K 106	P 2350/3	O 26/2	R 2351/1	PR 90/1	O 24/2a	PR 26/2
Eu	1	2.8	0.8	0.6	1.3	1.3	1.8	2	2	2.4	0.5	0.1	1.5	3	2
Gd	17	100	10	5	35	22	100	34	55	100	5.5	0.6	40	230	85
Tb	2	30	0.5	1	3	1	200	3	3	1.5	2	0.5	1	0.5	0.5
Dy	7	13	3.2	3.8	7.5	4.3	13	8.5	9	7.3	5	0.3	10	22	12
Ho	1.8	5	3	0.7	2.2	0.7	8	1.2	2.8	2.2	0.8	0.2	3.2	15	4.4
Er	5	10	10	1.5	4.6	1.5	11	3.2	7	3.4	3	0.4	8	40	9
Tm	0.5	1.5	0.8	1.8	0.6	0.15	1.5	0.4	0.8	0.6	0.34	0.05	1	5	0.75
Yb	1.7	5	7	1.1	1.8	0.9	2.5	1.5	2.3	1.7	1.5	0.4	2.5	5.3	1.8
Lu	0.2	0.4	0.2	0.2	0.24	0.12	0.6	0.24	0.5	0.34	0.2	0.02	0.5	1.5	0.2
Y	15	56	8.5	8.5	23	13	23	15	180	10	13	5	17	40	17
Zr		418	320	912	507	—	36	527	209	—	571	—	582	2500	476
Hf	6	4	1	35	6	3	14	8	1	80	21	1	3	170	4
Ta	3.8	3.8	2.1	1.7	3.5	2.5	3.5	7	12	7	3.3	5	2.2	14	5.2
Nb	4.	50	180	12	100	12	120	100	37	200	38	1.5	80	360	140
Be	50	30	5	10	30	10	15	10	3	50	2	5	1	20	20

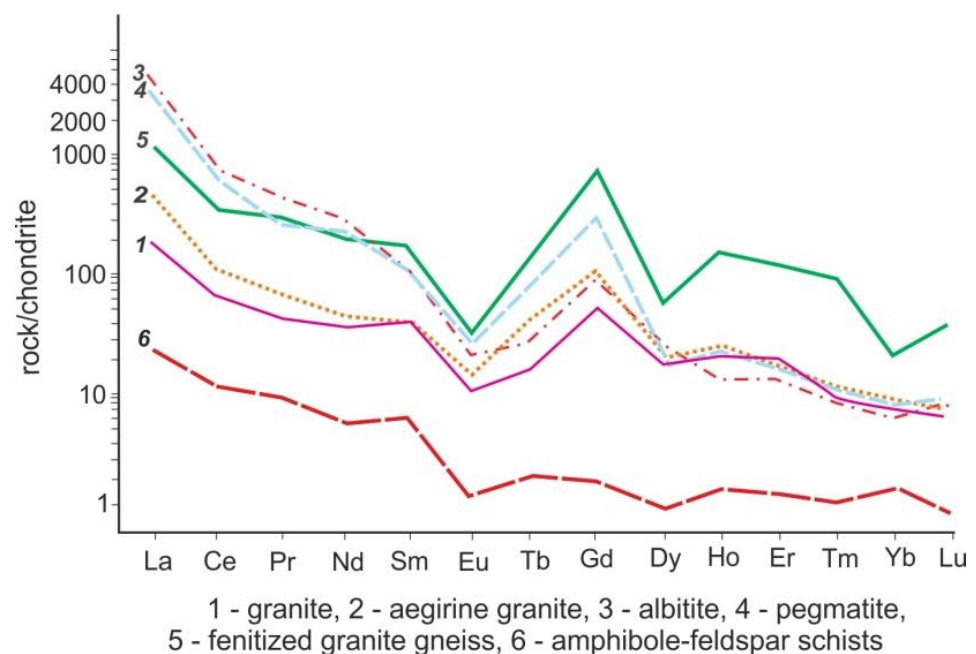


Figure 17. Chondrite-normalized [66] REE distribution patterns for the rocks of the Tømmot ore field.

Major ore bodies of the deposit are localized in finitized albitites and pegmatites. Table 5 shows the distribution of REEs in them. It is easy to see that the principal ore elements are Ce and Y, and other metals are present in subordinate quantities. Thus, the deposit can be classed as a complex Y-Ce deposit.

Table 5. Average composition of ores of the Tømmot deposit (in wt%).

Ore Body	HREE Total	La ₂ O ₅	Ce ₂ O ₃	Yb ₂ O ₃	Y ₂ O ₃	ThO ₂	ZrO ₂	Ta ₂ O ₅	Nb ₂ O ₅	BeO
1	0.5	0.09	0.16	—	0.58	0.03	0.4	0.05	—	—
2	0.23	0.09	0.63	—	0.82	—	—	—	—	—
3	0.22	0.37	3.13	0.025	3.99	—	—	0.015	0.05	0.017
4	1.18	0.5	4.4	0.28	1.01	1.55	0.88	0.016	0.25	0.38
5	1.06	0.12	0.61	0.82	0.32	0.044	0.32	0.02	0.09	0.002
13	3.63	0.53	1.01	0.002	0.66	0.048	0.38	0.003	0.13	0.076
16	1.04	0.12	0.2	0.23	0.06	0.06	0.97	—	0.1	0.003
17	3.24	0.22	1	—	0.7	0.23	0.37	0.001	0.01	0.15

6. Discussion

The Tommot massif is composed of a complex of alkaline rocks with a varying composition, from jacupirangites to alkaline syenites. Field studies have revealed the intrusion of the ultrabasic rocks by gabbroids and syenites and the basic rocks by syenites. Additionally, the presence of ultrabasic rock xenoliths in gabbro and gabbro xenoliths in syenites was observed. The results of isotope dating confirm the established sequence of the massif formation. In the petrochemical diagrams, the data points of the massif rocks form a common trend (Figures 8 and 9). With a transition from the ultrabasic rocks to syenites, $\text{FeO}^*/(\text{FeO}^* + \text{MgO})$ and $\text{Al}_2\text{O}_3/(\text{FeO}^* + \text{MgO})$ values, the sum of alkalis, and differentiation indices increase with silica content, whereas the temperature of the melts and the depth of magma generation decline. These data suggest that the massif rocks are derivatives of three successive stages (or phases) of the intrusion of a single melt or some genetically related melts [27]. The maximum calculated temperatures and pressures during the parent melt generation were 1300–1400 °C and 30 kbar for ultrabasic rocks, 1100–1200 °C and 20–25 kbar for basic rocks, and 1000 °C and 16–18 kbar for syenites.

Among the ultrabasic and basic rocks of the Tommot massif, rocks of normal alkalinity are sporadically present (Figures 8 and 18). Olivines of the ultrabasic rocks and some clinopyroxenes of the ultrabasic and basic rocks correspond to those from continental ultrabasic and basic rocks of normal alkalinity. The calculated PT conditions of crystallization indicate the initiation of a magma chamber in the upper mantle. Low values of $(^{87}\text{Sr}/^{86}\text{Sr})_0$ (0.7024–0.7028) suggest the generation of the ultrabasic melt in the depleted mantle. At the same time, Sr-isotopic disequilibrium has been established for minerals of the ultrabasic rocks (magnetite from jacupirangite) and gabbroids (plagioclases) ($(^{87}\text{Sr}/^{86}\text{Sr})_0 = 0.7028\text{--}0.7047$ and $(^{87}\text{Sr}/^{86}\text{Sr})_0 = 0.7027\text{--}0.7050$, respectively). According to [27], a probable reason for this and the growing $(^{87}\text{Sr}/^{86}\text{Sr})_0$ value in syenites (0.7054 ± 0.0011) is the interaction of the evolving parental melt with deep-seated fluids enriched with lithophile elements and radiogenic Sr. The La/Yb–Yb ratios also indicate the generation of the ultrabasic melt in a depleted or slightly metasomatized mantle and the increasing degree of mantle metasomatism during the formation of gabbroids and syenites (Figure 19).

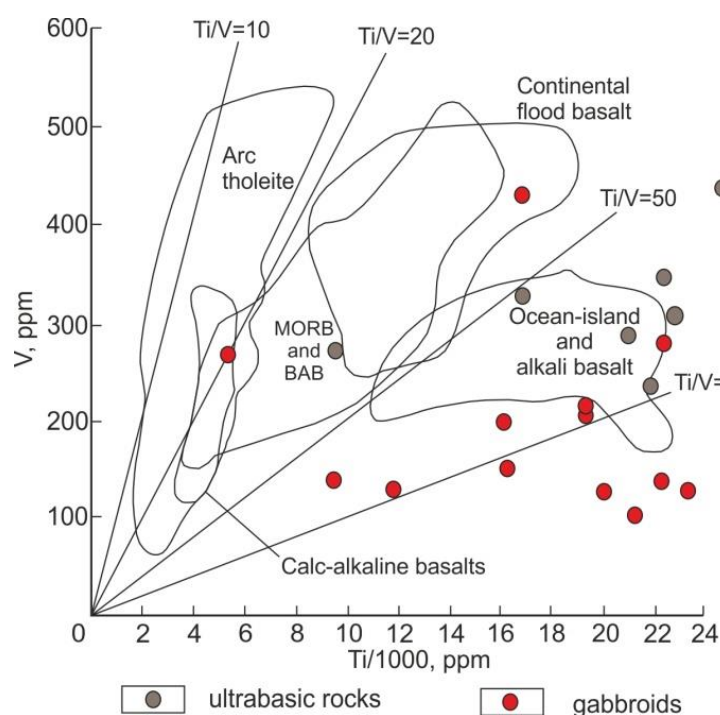


Figure 18. V vs. Ti/1000 diagram for ultrabasic and basic rocks of the Tommot massif. Fields and trends after [67].

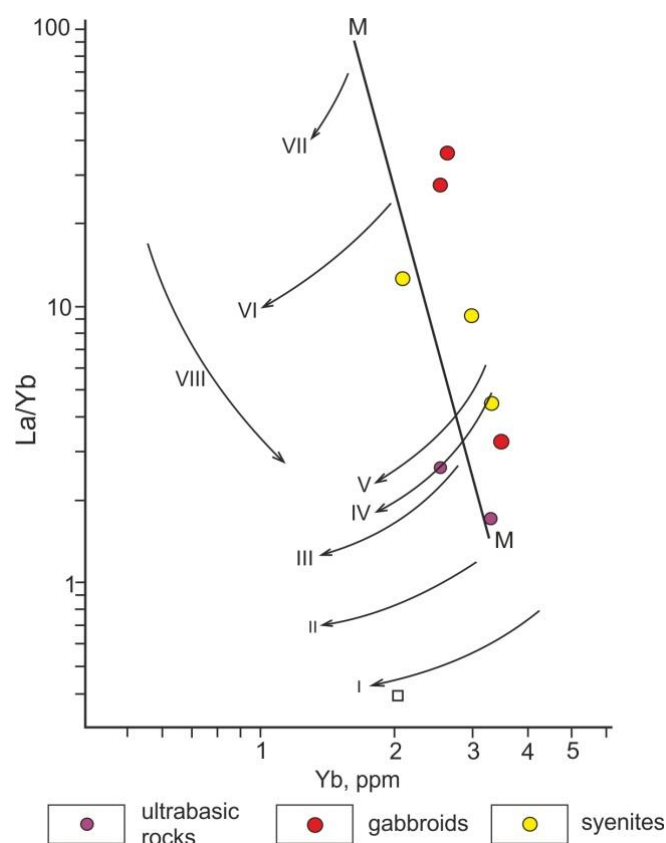


Figure 19. La/Yb vs. Yb diagram for igneous rocks of the Tommot massif. Differentiation trends [68]: I—depleted plagioclase lherzolites, II—depleted spinel lherzolites, III–V—primitive spinel lherzolites, VI and VII—metasomatically enriched lherzolites, M–M—trend of mantle enrichment.

The chemical compositions of the Somnitelnyi massif rocks correspond to alkaline feldspar granites with deviations of syenogranites and quartz alkaline feldspar syenites (Figure 10). The granites are highly differentiated ($DI = 78.5\%–95.3\%$) and highly ferruginous ($FeO^*/(FeO^* + MgO) = 89\%–99\%$). Their least modified varieties are metaluminous and acmite-normative. In most of the discrimination diagrams, their data points form a trend independent of the main evolutionary trends, which is typical for A-type granites. The geochemical features of the rocks and the presence of alkaline minerals (kaersutite, arfvedsonite, aegirine) in the granites also prove their affinity to A-type granites (Figures 13, 14 and 16).

There is no direct data available on the composition of the magma-generating substrate for the Somnitelnyi granites. The thickness of the Earth's crust in the study area is 36–38 km [23,69]. The maximum estimated depth of magma generation corresponds to $P = 9.5$ kbar (about 30 km) [55]. The calculated pressure at the pyroxene crystallization is 8–10 kbar (Table S1). Among the studied zircons, there is a generation of crystals identical in composition to zircons of eclogites and charnockites. Hence, it can be assumed that generation of the granite melt occurred in the lower crust. The maximum temperature of magma generation is 1045 °C [54]. The crystallization temperature interval determined for the granites with the use of GCDkit software [21] is 1030–742 °C (zircon- and apatite-saturation temperatures), and from mineral geothermometry it is 1027–640 °C at a pressure within 9.1–0.86 kbar. A high zircon-saturation temperature is considered one of the most characteristic features of A-type granites. For such granites from different regions of the world, this temperature is estimated at 800–1000 °C [70,71]. For different granite samples of the Somnitelnyi massif, it is 1027–990 °C. The petro- and geochemical signatures of the Somnitelnyi granites indicate they were formed in a within-plate rift-related geody-

namic setting (Figures 11 and 15), which is also typical for alkaline granites—the most high-temperature of all A-type granites.

The problem of the genesis of A-type granites is the most controversial to date. Several genetic models are proposed: deep differentiation of the initial basaltic or andesitic magma, crust anatexis, mixing or mingling of basic and silicic melts, and metasomatic fenitization of magma-generating substrates [70–73]. Most researchers, following G.N. Eby [70], distinguish two genetic varieties of A-type granites: A₁-group granites formed from basalts of oceanic islands, continental rifts, and hot spots, and A₂-group granites are postcollisional, postorogenic, or anorogenic granites originated from basalts of island arcs and continental margins, or a crustal tonalite–granodiorite source, or by partial melting of the crust. In the Yb/Ta–Y/Nb and Ce/Nb–Y/Nb discrimination diagrams [70] (Figure 20), a significant part of the data points for the studied granites are localized within or near the OIB field corresponding to the A₁-group granites. The Y–Nb–Ce ratios in the rocks and the ratios between major petrogenetic oxides are also inherent in the A₁-group granites (Figure 21). However, in the DI–SiO₂ diagram, the data points for the granites fall into the field of crustal melt derivatives (Figure 22).

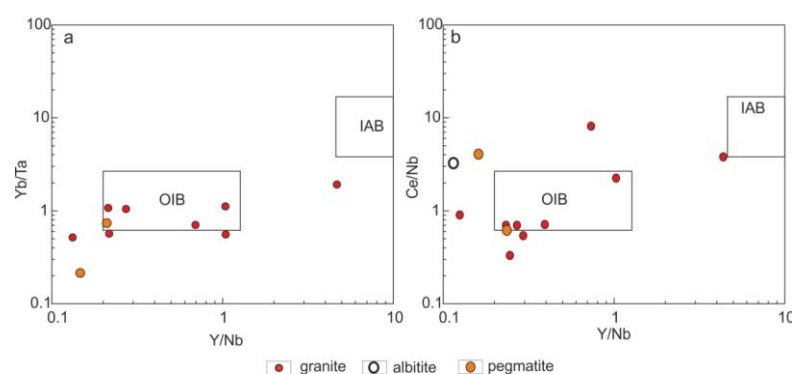


Figure 20. Yb/Ta vs. Y/Nb (a) and Ce/Nb vs. Y/Nb (b) diagrams for rocks of the Somnitelnyi massif and Tommot deposit. Fields in the diagram [70]: OIB—field of oceanic island basalts; IAB—field of granites formed from basalts of island arcs and continental margins or by partial melting of the crust.

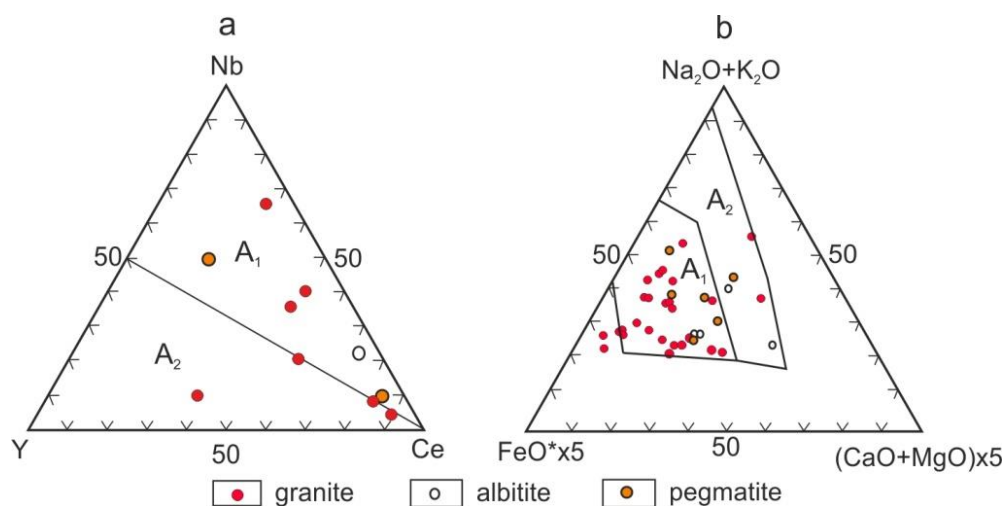


Figure 21. (a) Y–Nb–Ce and (b) (FeO* × 5) – (Na₂O + K₂O) – ((CaO + MgO) × 5) diagrams for rocks of the Somnitelnyi massif and Tommot deposit. Fields in the diagrams: (a) A₁—granitoids from rift, plume, and hotspot environments, A₂—granitoids from postcollisional, postorogenic, and anorogenic environments [70]; (b) A₁—silicic rocks of within-plate geodynamic settings: oceanic islands and continental rifts; A₂—felsic igneous rock associations of intracontinental- and continental-margin geodynamic settings [74].

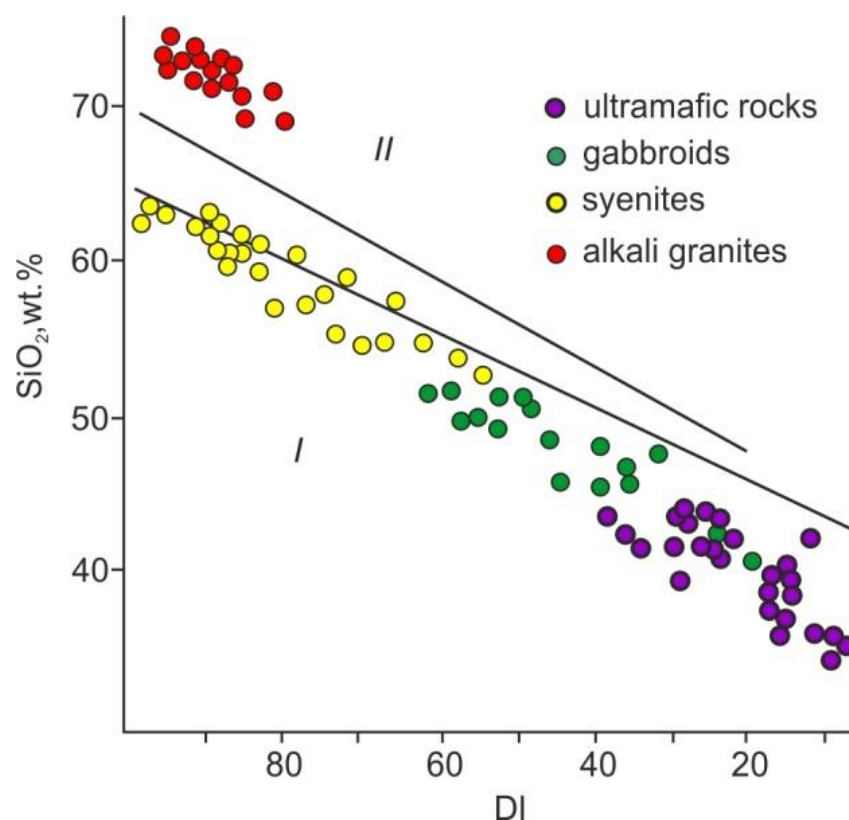


Figure 22. SiO₂ vs. DI diagram for igneous rocks of the Tommot and Somnitetnyi massifs. Fields in the diagram after [53]: I—derivatives of mantle melts, II—derivatives of crustal melts.

The crustal origin of the parent melt is also supported by a high ($^{87}\text{Sr}/^{86}\text{Sr}$)₀ value (0.7441 ± 0.0083) [27] and the calculated depths of magma generation. A high temperature of the granitic melt at a relatively low pressure could only be reached with the involvement of mafic magmas or/and hot mantle fluids. The majority of researchers involved in the study of A-type granites have come to the same conclusion. This is particularly true for the formation of the most high-temperature alkaline granites [70,75,76].

As compared with the primitive mantle and crust, the granites of the Somnitetnyi massif are highly enriched with Rb, K, Zr, and almost all REEs, with the exception of Yb and Lu (Table 3, Figure 17). The spectral quantitative analysis showed they are also high in Cr, Ni, and V. On the spidergrams [77] (Figure 23), the Sr, P, and Ti minima are clearly seen, which is characteristic of crustal rocks as distinct from those derived from mantle magmas [78]. On the other hand, the enrichment of REEs and Zr is typical precisely for alkaline granites formed from OIB-like sources [17,70,79]. These contradictions can be explained by the magma generation in the crust under the action on the crustal substrates of juvenile solutions derived from the metasomatized mantle, which were enriched with alkalis and ore elements [76,80,81].

A number of researchers consider the Somnitetnyi massif granites to be the fourth phase of magmatism, following the third-phase syenites [82]. However, although isotopic ages of the rocks of different phases of the Tommot massif are relatively close, there is a long time gap between the formation of the Tommot syenites and the Somnitetnyi granites, estimated by different methods at 112 to 160 Ma, which is inconsistent with the assumption of their origin from a single evolving melt. The fact that the data points for the Somnitetnyi granites and the rocks of the Tommot massif occupy different positions in all discrimination petrochemical diagrams does not agree with this assumption either. The contents of almost all REEs (except for Sm, Eu, and Tb) and Hf, which are the most characteristic elements of the metasomatized mantle [83], increased over time from ultrabasic rocks to syenites to granites. The growth was smooth for the rocks of the Tommot massif and sharp for the

Somnitelnyi granites. In the ultrabasic rocks of the Tommot massif only single grains of REE minerals (chevkinite, bastnasite, thorite) were found, and in gabbroids and syenites, rare grains of chevkinite, monazite, and allanite were noted. The main carriers of REEs in gabbroids and syenites are accessory zircons, the most abundant in alkaline and foid syenites. REE occurrences are mostly concentrated in the near exocontact of the Somnitelnyi massif and much less in its endocontacts. High REE contents are characteristic for fenitized granite gneisses, schists, and fenitized albitites, with maximum values observed in fenitized albitites and cross-cutting pegmatites (Figure 17). Distribution patterns of trace elements for granites, albitites, and pegmatites are nearly the same (Figure 23), which once again emphasizes, at least, the paragenetic relationship of REE mineralization with the Somnitelnyi massif granites. Thus, the Tommot deposit can be referred to as a complex metasomatic deposit related to granosyenites and alkaline granites. The enrichment of the granites and postmagmatic solutions they produce with REEs and Hf could be due to generation of the parent melt for the granites in fenitized crustal substrates [71]. The fenitization processes are widely covered in the literature. The overwhelming majority of researchers associate them with the action of solutions generated by deep-seated alkaline melts [84].

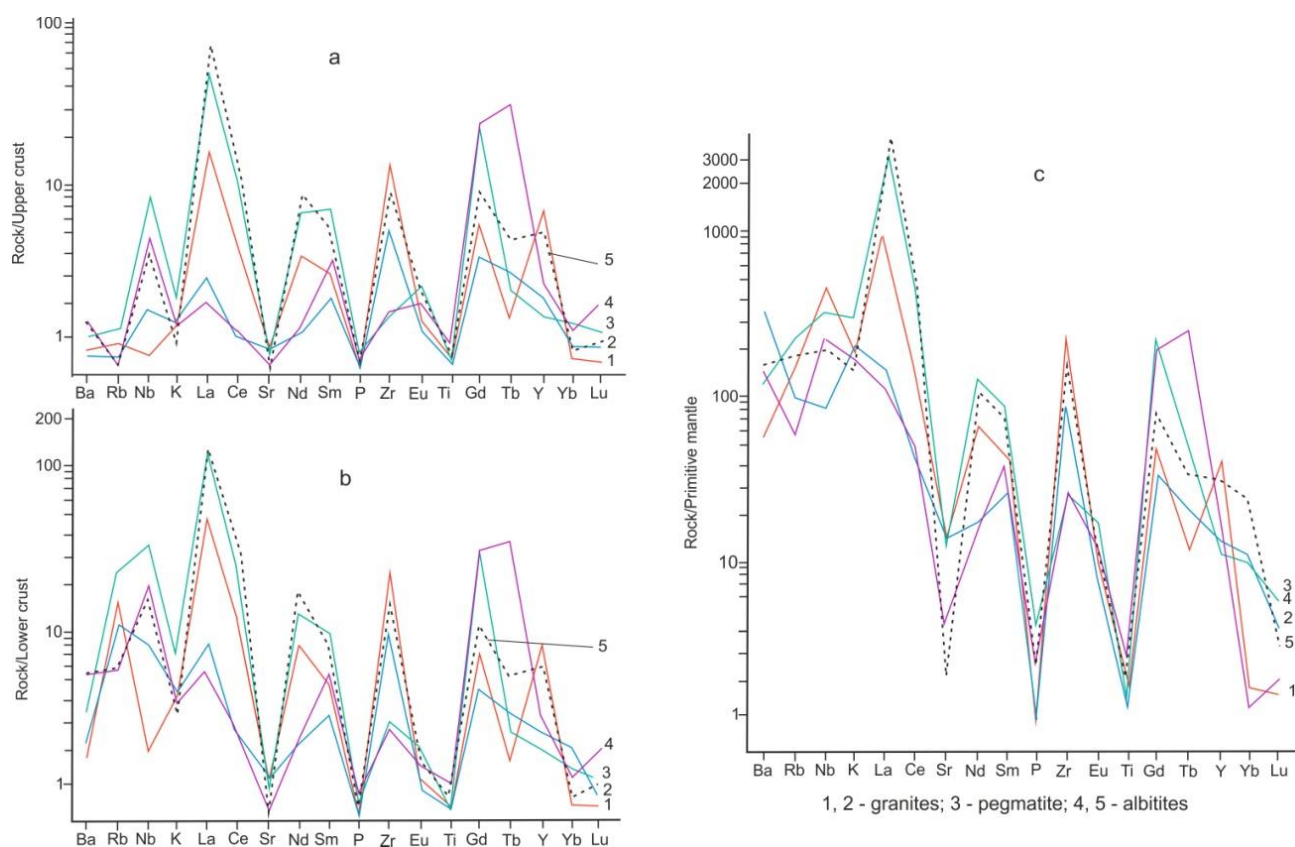


Figure 23. Upper crust- (a), lower crust- (b), and primitive mantle-normalized (c) [77] trace-element patterns for the rocks of the Somnitelnyi massif and Tommot deposit.

Large complex Ta-Nb-REE deposits (Katuginskoye, Ulug-Tanzekskoye, Zashikhinskoye, etc.) are associated with feldspar metasomatites, albitites, albitized alkaline granites, and syenites. Each of them has both common and specific features. For example, the fenitization processes also have been described from the large complex Verkhneye Espe Nb-Zr-REE deposit (Kazakhstan), where, just like at the Tommot deposit, the main ore bodies occur in albitites and fenites in exo- and endocontacts of the alkaline granite massif [85].

7. Conclusions

(1) A long-term evolution of magmatism within the Tommot ore field is confirmed, including the emplacement of the multiphase Tommot massif of varying compositions, from alkaline–ultrabasic rocks to alkaline syenites, and the Somnitelnyi massif of moderately alkaline and alkaline leucogranites and granites.

(2) The petro- and geochemical signatures of the granites, and their magma generation and crystallization parameters, as well as a long time gap between the formation of syenites and granites do not make it possible to interpret the Somnitelnyi massif granites as a final phase of the Tommot massif formation. However, all igneous rocks of the Tommot ore field bear traces of the impact of deep-seated solutions rich in alkalis and REEs; thus, this suggests a prolonged existence within the study area of a source of undepleted heated mantle (“hot spot”) whose maximum activity took place during the granitic melt generation. This is also proved by the established affinity of the Somnitelnyi massif granites to A-type (A₁-group) granites, whose generation is impossible without the mixing of magma-generating substrates with deep-seated fluids.

(3) The REE mineralization occurs in exocontacts and, less often, endocontacts of the Somnitelnyi granite, and is not found in the host rocks and in the inner part of the massif away from the contacts. No significant mineralization is identified within the Tommot massif. The main ore bodies of the Somnitelnyi massif consist of fenitized albitites and pegmatites.

(4) The Tommot deposit was formed by postmagmatic solutions generated by the granitic melt.

Based on the data obtained, the Tommot deposit is classified as a metasomatic deposit related to the emplacement of subalkaline and alkaline granites. It is a complex Ce–Y deposit with accompanying Zr, Nb, and Th mineralization.

Supplementary Materials: The following supporting information can be downloaded at: <https://www.mdpi.com/article/10.3390/min12111347/s1>, Table S1: Contents of major elements (wt.%) in pyroxenes of the Tommot and Somnitelnyi massifs. Table S2: Contents of major elements (wt.%) in amphiboles of magmatic rocks of the Tommot and Somnitelnyi massifs. Table S3: Contents of major elements (wt.%) in biotites of magmatic rocks of the Tommot and Somnitelnyi massifs. Table S4: Contents of major elements (wt.%) in magmatic rocks of the Tommot massif. Table S5: Contents of major elements (wt.%) in magmatic rocks of the Somnitelnyi massif.

Author Contributions: Conceptualization, V.A.T. and A.V.P.; formal analysis, V.A.T. and A.V.P.; investigation, V.A.T. and A.V.P.; methodology, V.A.T.; writing—original draft, V.A.T.; writing—review & editing, A.V.P. All authors have read and agreed to the published version of the manuscript.

Funding: This study was supported by the project of the DPMGI SB RAS (FUEM-2019-0001). Interpretation of isotopic data was partly supported by the Russian Science Foundation (grant No. 20-17-00169).

Data Availability Statement: Not applicable.

Acknowledgments: The authors express gratitude to all who performed analytical research. Special thanks are due to M.I. Ivanov for his help in preparing the graphic material. We thank three anonymous reviewers for their constructive comments, suggestions, and corrections, which very much helped to improve the manuscript.

Conflicts of Interest: The authors declare no conflict of interest.

References

1. Balashov, Y.A. *Geochemistry of Rare Earth Elements*; Nauka: Moscow, Russia, 1976; p. 267. (In Russian)
2. Semenov, E.I. *Ore and Mineralization of Rare Earths, Thorium and Uranium (Lanthanides and Actinoids)*; Geos: Moscow, Russia, 2001; p. 307. (In Russian)
3. Mariano, A.N. Economic geology of Rare Earth Minerals. In *Geochemistry and Mineralogy of Rare Earth Elements*; Lipin, B.R., McKay, G.A., Eds.; Mineralogical Society of America: Washington, DC, USA, 1989; pp. 309–337.

4. Long, K.R.; Van Gosen, B.S.; Foley, N.K.; Cordier, D. *The Principal Rare Earth Elements Deposits of the United States—A Summary of Domestic Deposits and A Global Perspective*; Scientific Investigations Report 2010–5220; U.S. Geological Survey: Reston, VA, USA, 2010; p. 104.
5. Eremin, N.V. *Strategic, Scarce and Critical Mineral Raw Materials (Rare Earth Elements)*; MSU Geofak: Moscow, Russia, 2020; pp. 26–47. (In Russian)
6. Mikhailov, V.A. *Rare Earth Ores of the World: Geology, Resources, Economics*; Kiev University: Kiev, Ukraine, 2010; pp. 49–134. (In Russian)
7. Trunilina, V.A. Late Cretaceous Granites of the Selennyakh Ridge (Verkhoyansk-Kolyma Orogenic Area). *Solid State Technol.* **2020**, *63*, 4501–4525.
8. Nédélec, A.; Bouchez, J.L. *Granites: Petrology, Structure, Geological Setting, and Metallogeny*; University Press: Oxford, UK, 2015; p. 349.
9. Dehaine, Q.; Filippov, L.O.; Glass, H.J.; Rollinson, G. Rare-metal granites as a potential source of critical metals: A geometallogical case study. *Ore Geol. Rev.* **2019**, *104*, 384–402. [CrossRef]
10. Melcher, F.; Graupner, T.; Gäbler, H.E.; Sitnikova, M.; Henjes-Kunst, F.; Oberthür, T.; Gerdes, A.; Dewaele, S. Tantalum–(niobium–tin) mineralisation in African pegmatites and rare metal granites: Constraints from Ta–Nb oxide mineralogy, geochemistry and U–Pb geochronology. *Ore Geol. Rev.* **2015**, *64*, 667–719. [CrossRef]
11. Huang, H.; Wang, T.; Zhang, Z.; Qin, Q. Petrogenesis and rare metal mineralization of the alkaline granitic magma: A case study from the Boziguo’er rare metal granitic intrusion. *Geodyn. Tectonophys.* **2017**, *8*, 475–476. [CrossRef]
12. Kovalenko, V.I.; Yarmolyuk, V.V.; Kozlovsky, A.M.; Kovach, V.P.; Sal’nikova, E.B.; Kotov, A.B.; Vladyskin, N.V. Two types of magma sources of rare-metal alkali granites. *Geol. Ore Deposits* **2020**, *49*, 442–466. [CrossRef]
13. Xu, X.; Zhou, X.; Wang, D. Interaction crust–mantle and genesis of granites on the matter of coastal part of the south-eastern part of China. *Geol. I. China Univ.* **1999**, *5*, 241–250.
14. Sami, M.; Mahdy, N.M.; Ntaflos, T.; Fathy, D. Composition and origin of Ti–Nb–Ta–Zr bearing minerals in the Abu Diab highly evolved granite from the Central Eastern Desert of Egypt. *J. Afr. Earth Sci.* **2020**, *165*, 103808. [CrossRef]
15. Collins, W.J.; Beams, S.D.; White, A.J.R.; Chappell, B.W. Nature and origin of A-type granites with particular reference to Southeastern Australia. *Contrib. Mineral. Petrol.* **1982**, *80*, 189–200. [CrossRef]
16. Vladimirov, A.G.; Vystavnoy, S.A.; Titov, A.V.; Rudiev, S.N.; Dergachev, V.B.; Annikova, I.Y.; Tikunov, Y.V. Petrology of the Early Mesozoic rare-metal granites of the southern Altai Mountains. *Geol. Geophys.* **1998**, *7*, 901–916. (In Russian)
17. Bonin, B. A-type granite ring complexes: Mantle origin through crustal filters and the anorthosite-rapakivi magmatism connection. *Petrol. Geochem. Mag. Suites Rocks Contin. Ocean. Crusts* **1996**, 201–217.
18. Abdel-Karim, A.; Azer, M.; Sami, M. Petrogenesis and tectonic implications of the Maladob ring complex in the South Eastern Desert, Egypt: New insights from mineral chemistry and whole-rock geochemistry. *Int. J. Earth Sci.* **2021**, *110*, 53–80. [CrossRef]
19. Kile, D.E. The Universal Stage: The Past, Present, and Future of a Mineralogical Research Instrument. *Geochem. News* **2009**, *140*, 1–21. Available online: <http://www.geochemsoc.org/publications/geochemicalnews/gn140jul09/theuniversalstage.htm> (accessed on 30 June 2009).
20. Saranchina, G.M.; Kozhevnikova, V.N. *Fedorov’s Method: Determination of Minerals, Microstructural Analysis*; Nedra: Leningrad, Russia, 1985; p. 208. (In Russian)
21. Janoušek, V.; Farrow, C.M.; Erban, V. Interpretation of whole-rock geochemical data in igneous geochemistry: Introducing Geochemical Data Toolkit (GCDkit). *Petrology* **2006**, *47*, 1255–1259. [CrossRef]
22. Korinevsky, E.V. Petroexplorer—a system for creating geochemical information and analytical arrays in the process of case studies. *Geoinformatika* **2015**, *4*, 48–53. (In Russian)
23. Parfenov, L.M.; Kuzmin, M.I. (Eds.) *Tectonics, Geodynamics and Metallogeny of the Territory of the Republic of Sakha (Yakutia)*; MAIK “Nauka/Interperiodika”: Moscow, Russia, 2001; p. 571. (In Russian)
24. Nokleberg, W.J. (Ed.) *Metallogenesis and Tectonics of Northeast Asia*; U.S. Geological Survey Professional Paper 1765: Washington, DC, USA, 2010; p. 624.
25. Layer, P.W.; Parfenov, L.M.; Surnin, A.A.; Timofeev, V.F. First $^{40}\text{Ar}/^{39}\text{Ar}$ age determinations of magmatic and metamorphic rocks of the Verkhoyansk-Kolyma Mesozoides. *Doklady RAN* **1993**, *329*, 621–624. (In Russian)
26. Gorbov, G.S.; Zhukhina, I.A. The first definitions of the absolute age of metamorphic rocks of the Kolyma massif. *Doklady AN SSSR* **1971**, *197*, 1131–1132. (In Russian)
27. Trunilina, V.A.; Layer, P.W.; Parfenov, L.M.; Zaitsev, A.I.; Orlov, Y.S. The Tommot Massif: A middle Paleozoic rift-related alkaline gabbro and syenite complex, Yakutia, northeast Russia. *Stephan Mueller Spéc. Publ. Ser.* **2009**, *4*, 97–109. [CrossRef]
28. Solodov, N.A. *Predictive Prospecting Complexes for the Main Geological and Industrial Types of Rare Metals Deposit*; IMGRE: Moscow, Russia, 1989; p. 245. (In Russian)
29. Kalinin, M.A.; Molchanov, A.V.; Terekhov, A.V.; Mikhailov, V.A.; Afanasyeva, E.V. Platinum bearing of the Tommot massif (north-eastern Yakutia). In *Collection of Abstracts Mineral Resource Base of Diamonds, Precious and Non-Ferrous Metals—from Forecast to Production*; IMGRE: Moscow, Russia, 2021; pp. 68–75. (In Russian)
30. Le Maitre, R.W. (Ed.) *Igneous Rocks. A Classification and Glossary of Terms*; University Press: Cambridge, UK, 2002; p. 253.
31. Ryabov, V.V.; Zolotukhin, V.V. Clinopyroxene. In *Minerals of Differentiated Traps*; Sobolev, V.S., Ed.; Nauka: Novosibirsk, Russia, 1977; pp. 37–70. (In Russian)
32. Putirka, K.D. Thermometers and barometers vor volcanic systems. *Rev. Mineral. Geochem.* **2008**, *69*, 61–120. [CrossRef]

33. Yavuz, F. Win Pyroxene: A Windows program for pyroxene calculation classification and thermobarometry. *Amer. Miner.* **2013**, *98*, 1338–1359. [[CrossRef](#)]
34. Rudolphi, R.; Renzulli, A. Calcic amphiboles in calc-alkaline and alkaline magmas: Thermobarometric and chemometric empirical equations valid up to 1130 °C and 2,2 Gpa. *Contrib. Miner. Petrol.* **2012**, *163*, 877–895. [[CrossRef](#)]
35. Yavuz, F. *A Program to Classify Microprobe and Wet Chemical Amphibole Analyses according to the IMA (1997) Nomenclature Scheme*; AGU: Istanbul, Turkey, 1999.
36. Uchida, E.; Endo, S.; Makino, V. Relationship between solidification depth of granitic rocks and formation of hydrothermal ore deposits. *Resour. Geol.* **2007**, *57*, 47–56. [[CrossRef](#)]
37. Henry, D.A.; Guidotti, C.V.; Thompson, J.A. The Ti-saturation surface for low- to-medium pressure metapelitic biotites: Implication for geothermometry and Ti-substitution mechanism. *Amer. Miner.* **2005**, *90*, 316–328. [[CrossRef](#)]
38. Troshin, Y.P.; Grebenshikova, V.I.; Antonov, A.Y. Volatile components in biotites and metallogenic specialization of intrusions. In *Mineralogical Criteria for Ore Content Assessment*; Nauka: Leningrad, Russia, 1981; pp. 73–83. (In Russian)
39. Tindle, A.G.; Webb, R.P. Estimation of lithium contents in trioctahedral micas using microprobe data: Application to micas from granitic rocks. *Eur. J. Miner.* **1990**, *2*, 595–610. [[CrossRef](#)]
40. Putirka, K.D. Igneous thermometers and barometers based on plagioclase + liquid equilibria: Tests of some existing models and new calibrations. *Amer. Miner.* **2005**, *90*, 336–346. [[CrossRef](#)]
41. Bushlyakov, I.N.; Kholodnov, V.V. *Halogens in Petrogenesis of Granitoids*; Nedra: Moscow, Russia, 1986; p. 192. (In Russian)
42. Gusev, A.I. Typification of granitoids, based on biotite composition. *Achiev. Mod. Nat. Sci.* **2009**, *4*, 54–57. (In Russian)
43. Brimhall, G.H.; Crerar, D.A. Ore fluids: Magmatic to supergene. In *Thermodynamic Modeling of Geological Materials. Minerals, Fluids and Melts*; Reviews in Mineralogy and Geochemistry: Lansing, MI, USA, 1987; Volume 17, pp. 235–321.
44. Krasnobaev, A.A. *Zircon as an Indicator of Geological Processes*; Nauka: Moscow, Russia, 1986; p. 202. (In Russian)
45. Corfu, F.; Hanchar, J.M.; Hoskin, P.W.O.; Kinny, P. Atlas of Zircon Textures. *Rev. Mineral. Geochem.* **2003**, *53*, 469–500. [[CrossRef](#)]
46. Rubatto, D. Zircon trace element geochemistry: Partitioning with garnet and the link between U-Pb ages and metamorphism. *Chem. Geol.* **2002**, *184*, 123–138. [[CrossRef](#)]
47. French, W.J.; Cameron, E.P. Calculation on the temperature of crystallization of silicates from basaltic melts. *Mineral. Mag.* **1981**, *44*, 19–26. [[CrossRef](#)]
48. Kulikova, V.V.; Kulikov, V.S. *Petrochemical Classification of Magmatic Rocks*; Kola Scientific Center: Petrozavodsk, Russia, 2001; p. 115. (In Russian)
49. Piskunov, B.M.; Abdurakhmanova, A.I.; Kim, C.U. Composition-depth ratio for volcanoes of the Kuril island arc and its petrological significance. *Volcanol. Seismol.* **1979**, *4*, 57–67. (In Russian)
50. Sharpenok, L.N.; Kostin, A.E.; Kukharensko, E.A. TAS-diagram sum of alkalis-silica for chemical classification and diagnostics of plutonic rocks. *Reg. Geol. Metallog.* **2013**, *56*, 40–50. (In Russian)
51. Borodin, L.S. *Petrochemistry of Magmatic Series*; Nauka: Moscow, Russia, 1987; p. 260. (In Russian)
52. Borodin, L.S. Model system of petrochemical and metallogenic trends of granitoids as a basis for the prognosis of Sn, Li, Ta, Nb, W, Mo, and Cu deposits. *Geol. Ore Depos.* **2004**, *46*, 3–26.
53. Thornton, C.P.; Tuttle, O.F. Chemistry of igneous rocks, differentiation index. *Am. J. Sci.* **1960**, *258*, 664–684. [[CrossRef](#)]
54. Jung, S.; Pfander, J.A. Source composition and melting temperatures of orogenic granitoids—constraints from CaO/Na₂O, Al₂O₃/TiO₂ and accessory mineral saturation thermometry. *Eur. J. Miner.* **2007**, *1*, 5–40.
55. Belyaev, G.M.; Rudnik, V.A. *Formational-Genetic Types of Granitoids*; Nedra: Leningrad, Russia, 1978; p. 168. (In Russian)
56. Strekeisen, A.; Le Maitre, P.W. A chemical approximation to the modal QAPF classification of igneous rocks. *Neues Jahrb. Miner.* **1979**, *136*, 169–206.
57. Maniar, P.D.; Piccoli, P.M. Tectonic discrimination of granitoids. *Geol. Soc. Am. Bul.* **1989**, *101*, 635–643. [[CrossRef](#)]
58. Frost, B.R.; Arculus, R.J. A geochemical classification for granitic rocks. *J. Petrol.* **2001**, *42*, 2033–2048. [[CrossRef](#)]
59. Maeda, J. Opening of the Kuril Basin deduced from the magmatic history of Central Hokkaido, northern Japan. *Tectonophysics* **1990**, *174*, 235–255. [[CrossRef](#)]
60. Datsenko, V.M. Petrogeochemical typification of granitoids of the south-western framing of the Siberian platform. In *Materials the Second All-Russian Petrographic Meeting, Syktyvkar, Russia, 27–30 June 2000*; Yushkin, N.P., Ed.; Komi Scientific Center: Syktyvkar, Russia, 2000; pp. 270–274. (In Russian)
61. Pearce, J.A.; Harris, N.B.W.; Tindle, A.G. Trace element discrimination diagrams for the tectonic interpretation of the granitic rocks. *J. Petrol.* **1984**, *25*, 956–963. [[CrossRef](#)]
62. Trunilina, V.A.; Roev, S.P.; Orlov, Y.S.; Oxman, V.S. *Magmatism of Various Geodynamic Environments (Zone of Junction of the Verkhoyansk Margin of the Siberian Continent and the Kolyma-Omolon Microcontinent)*; Yakut Scientific Center: Yakutsk, Russia, 1999; p. 168. (In Russian)
63. Ovchinnikov, L.N. *Applied Geochemistry*; Nedra: Moscow, Russia, 1990; p. 248. (In Russian)
64. Tauson, L.V. *Geochemical Types and Ore Potential of Granitoids*; Nauka: Moscow, Russia, 1977; p. 279. (In Russian)
65. Sazonova, L.V.; Nosova, A.A.; Dokuchaev, A.Y.; Gurbanov, A.G. Latite type of late collisional granitoids (North Caucasus): Geochemical and mineralogical features. *RAS Rep.* **2003**, *393*, 2–5. (In Russian)
66. Hofmann, A.W. Mantle geochemistry: The message from oceanic volcanism. *Nature* **1997**, *385*, 219–228. [[CrossRef](#)]
67. Shervais, J.W. Ti—V plots and the petrogenesis of modern and ophiolitic lavas. *Earth Planet. Sci. Lett.* **1982**, *59*, 101–118. [[CrossRef](#)]

-
68. Drill, S.I.; Kuzmin, M.I.; Tsipukova, S.S.; Zonenshain, L.P. Geochemistry of basalts from the West Woodlark, Lau and Manus basins: Implication for their petrogenesis and source rock composition. *Mar. Geol.* **1997**, *142*, 57–83. [[CrossRef](#)]
 69. Stogniy, G.A.; Stogniy, V.V. *Geophysical Fields of the Eastern Part of the North Asian Craton*; Yakutsk: Sakhapoligrafizdat, Russia, 2005; p. 173. (In Russian)
 70. Eby, G.N. Chemical subdivision of the A-type granitoids: Petrogenetic and tectonic implications. *Geology* **1992**, *20*, 641–644. [[CrossRef](#)]
 71. King, P.L.; White, A.J.R.; Chappell, B.W.; Allen, C.M. Characterization and Origin of aluminous A-type Granites from the Lachlan Fold Belt, Southeastern Australia. *J. Petrol.* **1997**, *38*, 371–391. [[CrossRef](#)]
 72. Litvinovsky, B.A.; Jahn, B.M.; Eyal, M. Mantle-Derived Sources of Syenites from the A-Type Igneous Suites—New Approach to the Provenance of Alkaline Silicic Magmas. *Lithos* **2015**, *232*, 242–265. [[CrossRef](#)]
 73. Wang, L.X.; Ma, C.Q.; Zhang, C. Halogen Geochemistry of IAnd A-Type Granites from Jiuhuashan Region (South China): Insights into the Elevated Fluorine in A-Type Granite. *Chem. Geol.* **2018**, *478*, 164–182. [[CrossRef](#)]
 74. Grebennikov, A.V. A-type granites and related rocks: Problems of identification, petrogenesis, and classification. *Russ. Geol. Geophys.* **2014**, *55*, 1074–1086. [[CrossRef](#)]
 75. Wu, F.Y.; Sun, D.Y.; Li, H.M. A-Type Granites in Northeastern China: Age and Geochemical Constraints on Their Petrogenesis. *Chem. Geol.* **2002**, *187*, 143–173. [[CrossRef](#)]
 76. Martin, R.F. A-Type Granites of Crustal Origin Ultimately Result from Open-System Fertilization-Type Reactions in an Extensional Environment. *Lithos* **2006**, *91*, 125–136. [[CrossRef](#)]
 77. Taylor, S.R.; Mc Lennan, S.M. *The Continental Crust: Its Composition and Evolution*; Blackwell: Oxford, UK, 1985; p. 384.
 78. Rudnick, R.L.; Gao, S. Composition of the Continental Crust. *Treatise Geochem.* **2003**, *3*, 1–64. [[CrossRef](#)]
 79. Shellnutt, J.G.; Zhou, M.F. Permian Peralkaline, Peraluminous and Metaluminous A-Type Granites in the Panxi District, SW China: Their Relationship to the Emeishan Mantle Plume. *Chem. Geol.* **2007**, *243*, 286–316. [[CrossRef](#)]
 80. Bogatkov, O.A.; Tsvetkov, A.A. *Magmatic Evolution of Island Arcs*; Nauka: Moscow, Russia, 1988; p. 249. (In Russian)
 81. Jahn, B.M.; Litvinovsky, B.A.; Zandvilevich, A.N. Peralkaline Granitoid Magmatism in the Mongolian-Transbaikalian Belt: Evolution, Petrogenesis and Tectonic Significance. *Lithos* **2009**, *113*, 521–539. [[CrossRef](#)]
 82. Nekrasov, I.Y. *Magmatism and Ore-Bearing Capacity of Northeastern Verkhoyansk-Chukotka Folded Area*; AN SSSR: Moscow, 1962; p. 334. (In Russian)
 83. Lesnov, F.P. *Rare Earth Elements in Ultramafic and mafic rocks and Their Minerals. Book 1 The Main Types of Rocks. Rock-Forming Minerals*; Geo: Novosibirsk, Russia, 2007; p. 401. (In Russian)
 84. Pirajno, F. *Hydrothermal Processes and Mineral Systems*; Springer: East Perth, Australia, 2009; p. 1273; ISBN 978-1-4020-8612-0.
 85. Baisalova, A.O. Features of Metasomatic Processes of Rare-Metal Manifestations of the Akzhailautas Granite Massif and Adjacent Areas. Ph.D. Thesis, Kazakh National Research Technical University, Alma-Aty, Kazakhstan, 2018. (In Russian)